The Pennsylvania State University
The Graduate School
College of Engineering

BIOMECHANICAL MODELLING OF TUMOR CLASSIFICATION AND GROWTH

A Thesis in
Engineering Mechanics
by
Antony J. Palocaren

Submitted in Partial Fulfillment
of the Requirements
for the Degree of

Master of Science

May 2011

The thesis of Antony Palocaren was reviewed and approved* by the following:

Corina Drapaca
Assistant Professor of Engineering Science and Mechanics
Thesis Advisor

Michael Lanagan
Professor of Engineering Science and Mechanics

Clifford Lissenden
Professor of Engineering Science and Mechanics

Judith A. Todd
P. B. Breneman Department Head Chair
Professor of Engineering Science & Mechanics

*Signatures are on file in the Graduate School.

Abstract:

Palpation is an important clinical diagnostic practice which is based on the fact that tumors tend to be stiffer than the surrounding normal tissue. None of the modern, non-invasive, imaging modalities (such as CT scan, Magnetic Resonance Imaging, or Ultrasound) used today by radiologists to find and diagnose tumors provides the critical information about the stiffness of the imaged tissues. The work presented in this thesis is based on the clinical observation of palpation and focuses on testing the following hypothesis: the Young's modulus of tissues helps differentiating not only between normal and abnormal tissues but, most importantly, between benign (not cancerous) and malignant (cancerous) tumors. We will show some preliminary results on tumor classification and growth with the help of biomechanical modeling. First, we propose a novel mechanical model of differentiating between benign and malignant tumors based on their corresponding Young's moduli obtained using information about tissue microstructure provided by imaging mass spectrometry. Imaging mass spectrometry is a new technology that can provide a molecular assessment of tumor progression and treatment obtained from biopsies, with the potential to identify tumor subpopulations and predict patient survival that is not evident based on the cellular phenotype determined histologically. Our second biomechanical model shows how the mechanical properties of tumors affect their growth. By replacing the first order temporal derivative in this mechano-growth model with a fractional order derivative we are able to predict for the first time when a benign tumor turns into cancer. We used the Adomian method to find analytic solutions to the non-linear classic and fractional-order ordinary differential equation corresponding to our second model.

Table of Contents

Acknowledgements:

I would like to thank all the people who have helped me, without whom this project would not have been possible: Dr. Corina Drapaca for her inspirational guidance and advising, my mom and dad for their continued support, and the Department of Engineering Science and Mechanics for giving me this opportunity.

Chapter 1

Introduction

1.1 Mechanical Properties of Biological Tissues

For centuries, palpation has been an important medical diagnostic tool. Palpation is the method of feeling for abnormalities in the body using your hands. The abnormalities can include tumors and bruises. The efficacy of palpation is based on the fact that many diseases can change the mechanical properties of tissues. These changes are caused either by the exudation of fluids from the vascular into the extra- and intercellular space or by loss of lymphatic systems, as in the case of cancer [37]. The result is an increase in stiffness or elastic modulus of the tissue. Even today surgeons try to feel for lesions during surgery that have been missed by a CAT scan, ultrasound or magnetic resonance. None of these scans can provide the information about the elastic properties of tissue elicited by palpation.

The elastic moduli of various human soft tissues are known to vary over a wide range, more than four orders of magnitude [37]. In contrast, most of the physical properties depicted by conventional medical imaging modalities are distributed over a much smaller numerical range. These observations have provided the motivation for many researchers to seek medical imaging technology that can estimate or assess the elastic moduli of tissues. The approaches to date have been to use conventional imaging

methods to measure the mechanical response of tissue to mechanical stress. The resulting strains have been measured using ultrasound, CT, or Magnetic Resonance Imaging (MRI) and the related elastic modulus has been computed from biomechanical models of tissues. In particular, the MR elastography method (MRE) using harmonic shear waves offers direct visualization and quantitative measurement of tissue displacements, high sensitivity to very small motions, a field of view unencumbered by acoustic window requirements, and the ability to obtain full three dimensional displacement information throughout a volume (see for example [19, 33, 37]).

In order to recover the mechanical properties of biological tissues we need to invert the displacement data measured using MRE. This inversion process requires the use of an accurate biomechanical model for tissues. It was noticed experimentally that most biological tissues have incompressible viscoelastic features: they have a certain amount of rigidity that is characteristic to solid bodies, and also they flow and dissipate energy by frictional losses as viscous fluids do. The incompressibility assumption for soft tissues is based on the fact that most tissues are made primarily of water. In addition, since the displacements in MRE are very small (order of microns), a linear constitutive law is usually assumed [37]. However, despite the richness of the data set, the variety of processing techniques and simplifications made in the biomechanical model, it remains a challenge to extract accurate results at high resolution in complex, heterogeneous tissues from the intrinsically noisy data. Therefore, any improvement in the MRE data processing with the help of biomechanics and computational methods will be of significant importance to modern medicine. MRE can help in tumor detection, determination of characteristics of disease, and in the assessment of rehabilitation.

1.2 Research Goals

The aim of this thesis is to formulate new biomechanical models that will be able to differentiate not only between normal and abnormal tissues, but more importantly, between benign and malignant tumors. As it can be seen in Fig.1-2.1, benign tumors

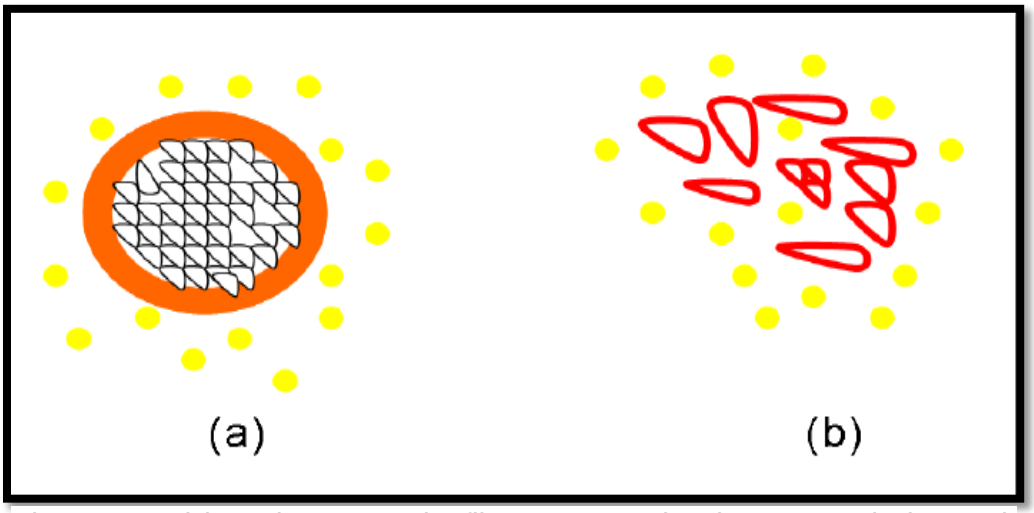

Figure 1-2.1 (a) Benign tumor: the fibrous connective tissue capsule (orange) separates the inside benign cells (black boundaries) from the outside normal cells (yellow). (b) Malignant tumor: the irregularly-shaped cancer cells (red boundaries) are diffusive and non-localized. [36] (inspired from [16])

tend to be more isotropic, and look more regularly shaped due in part to the presence of fibrous connective tissue shells that separate the benign tumors from the surrounding healthy tissue [12]. On the other hand, malignant tumors are diffusive, anisotropic and irregularly shaped. In order for the MRE method to correctly classify tumors as benign and malignant, the constitutive models of these two classes of tumors need to incorporate the chemo-mechanical differences between them. We believe that a more accurate formulation of the direct problem of MRE will help us not only to gain a better

understanding of the tumors' biomechanics but also to obtain more reliable elastic moduli by solving the inverse problem. Our objective is to link the mechanical and biochemical properties of biological tissues, and thus this research lies at the frontiers between engineering sciences, mechanics and medicine (more precisely, diagnostic radiology). In this thesis we propose first a novel biomechanical model for the Young's moduli of tumors that depend on the mass spectra of the proteins present in the tissues. *Our model shows that the Young's modulus of a high grade glioma is at least 10kPa higher than the Young's modulus of a low grade glioma.* In addition, we will use this model to investigate the effect of mechanics on the growth of tumors. The prediction of tumor growth is essential in treatment decision and planning. Our second mechano-growth model is a non-linear evolution differential equation which is solved analytically using the Adomian method. The time evolution is represented in two ways: (1) using a classic first-order derivative, and (2) using a fractional order derivative. The idea of using fractional order temporal derivatives to describe abnormal processes believed to be involved in the birth of tumors has been proposed in [59]. Unlike the classic integer order derivative, the fractional order derivative in our model appears to capture a very interesting temporal multi-scale effect of tumor transition from benign to cancer when a certain threshold of mechanical strain is reached in the tissue.

1.3 Human Impact of Research

Understanding the relationship between the mechanics and the biochemistry of biological tissues will have a tremendous impact on the development of advanced diagnostic and treatment clinical procedures. This work has the potential to play an

important role in developing better non-invasive imaging techniques capable not only to find but also to properly classify tumors, thus drastically reducing both - the very high health-related costs for medical diagnosis and treatments (economic component) and the number of deaths due to wrong diagnosis or delayed treatment (social component).

Chapter 2

Literature Review

In this chapter, we present a few fundamental concepts on mass spectroscopy, MR elastography, and tumor grading. The chapter ends with a very brief review of some biomechanical models for tumors existing in the literature.

2.1 Mass Spectroscopy

Mass spectroscopy is one of the most accurate methods for determining the elemental composition of a substance or a molecule [1-3]. The primary principle for this method is to ionize the substance or the chemical compound by bombarding it with high energy electrons (Fig. 2-1.1). As a result, positively charged fragments are produced and are accelerated in a vacuum through a magnetic field and are sorted on the basis of mass to charge ratio. Since the bulk of the ions produced in the mass spectrometer carry a unit positive charge, the value m/e is equivalent to the molecular weight of the fragment. We use this feature of mass spectroscopy to relate the Young's modulus to the concentration of proteins in the tissue. Tissue mass spectral analysis can be carried out through either a profiling or imaging approach. In the profiling approach, only specific locations within the tissue section are analyzed. In the imaging approach, protein distributions can be visualized over the entire tissue section. In recent years, mass spectrometry has become an indispensable tool for proteomic studies [1]. Desorption

and ionization techniques such as matrix-assisted laser desorption ionization mass spectrometry (MALDI MS) and electrospray ionization mass spectrometry (ESI MS) have literally revolutionized our ability to analyze proteins. These improvements offer levels of sensitivity and mass accuracy never before achieved for the detection, identification and structural characterization of proteins. It is now possible to routinely measure molecular weights above 200 kDa as well as obtain low parts per million mass measurement accuracies for the determination of peptides and proteins. Protein identification has been greatly facilitated because of the rapid expansion of protein and gene databases. Modern mass spectrometers can now rapidly map and fragment peptides that result from protease digestion in order to obtain sequence information and identify proteins [2]. MALDI MS is an ideal tool to investigate complex protein mixtures. It utilizes a matrix, a small acidic aromatic molecule that absorbs energy at the wavelength of the irradiating laser. The analyte molecule is mixed with the matrix in a ratio of typically 1/5000, deposited on a target plate and allowed to dry. During the drying process, matrix-analyte cocrystals form. These crystals are then submitted to very short laser pulses (typically UV laser light), resulting in desorption and ionization of the analyte molecule. Mostly intact protonated molecular ions are formed ([M+H], where M is the molecular weight of the analyte molecule). The mass-to-charge (*m/z*) of the ion is typically measured in a time-of flight mass analyzer [3].

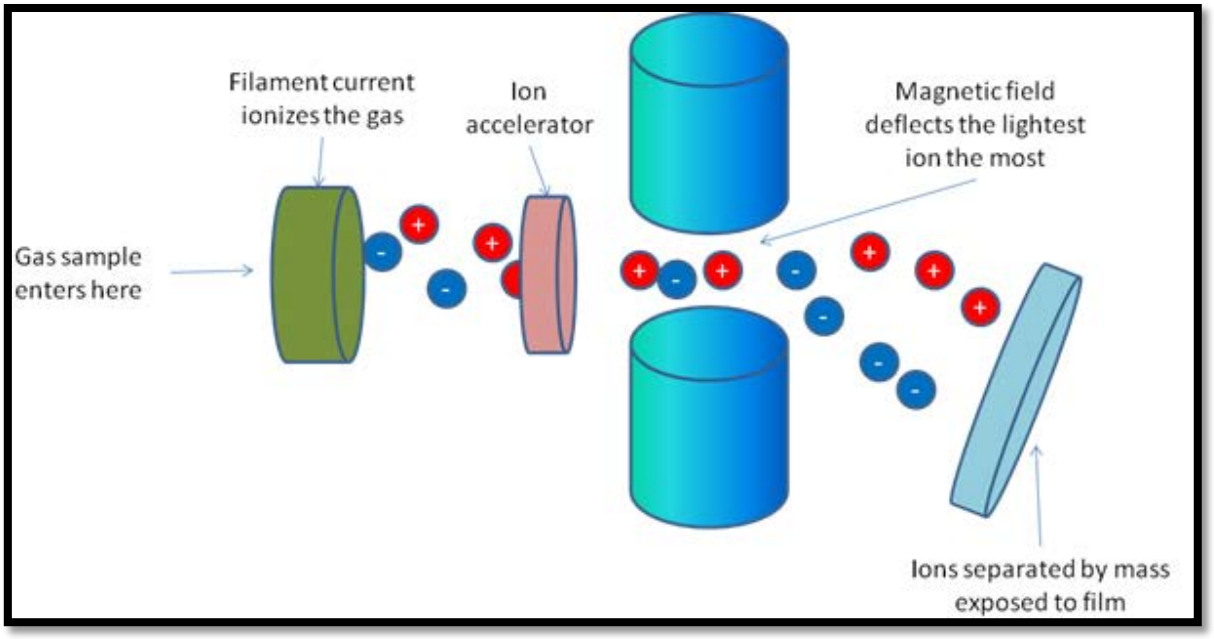

Figure 2-1.1 Classic mass spectroscopy setup.

One of the recent applications of MALDI MS is its use to profile and image proteins directly from thin tissue sections. MALDI imaging mass spectrometry (IMS) is a new technology that allows for simultaneous mapping of hundreds of peptides and proteins present in thin tissue sections with a lateral resolution of about 30–50 μm. Matrix is first uniformly deposited over the surface of the section, utilizing procedures optimized to minimize protein migration. Proteins are then desorbed from discrete spots or pixels upon irradiation of the sample in an ordered array or raster of the surface. Each pixel thus is keyed to a full mass spectrum consisting of signals from protonated species of molecules desorbed from that tissue region. A plot of the intensity of any one signal produces a map of the relative amount of that compound over the entire imaged surface. This technology provides an extremely powerful discovery tool for the investigation of biological processes [4-7, 10].

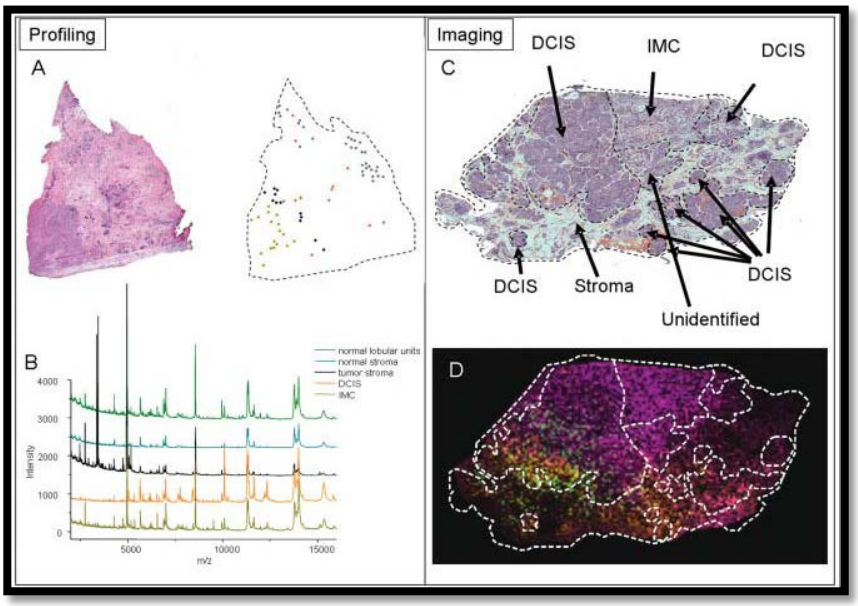

Figure 2-1.2: Profiling versus IMS demonstrated on human breast cancer tissue [18].

Direct tissue mass spectral analysis can be carried out through either a “profiling” or an “imaging” approach. In the profiling approach, only specific locations within the tissue section are analyzed often correlated with classical histology. In the imaging approach, protein distributions can be visualized over the entire tissue section. These processes are illustrated in Fig.2-1.2. In the profiling approach, matrix is deposited in discrete locations according to cell type to be analyzed across the tissue section, (Fig. 2-1.2A), and distinct mass spectra are obtained from each matrix spot (Fig. 2-1.2B). In the imaging approach, the matrix is deposited robotically in an array or uniformly coated across the tissue section, (Fig. 2-1.2C) and mass spectra are acquired systematically and are reconstructed into 2-D false color ion-density images (Fig. 2-1.2D).

In conclusion, the result of the profiling mass spectroscopy is a plot of the relative concentration (intensity) of the proteins found in the tissue versus the mass-to-charge ratio. On the other hand, image mass spectroscopy gives a map of the proteins' densities in the tissue. More details on image mass spectroscopy can be found, for instance, in [10, 18].

2.2 Magnetic Resonance Elastography

An elastogram is a mapping of material parameters (the Young's modulus, for example) in an anatomically meaningful image. The approaches to date have been to use conventional imaging methods to measure the mechanical response of tissue to mechanical stress. The resulting strains have been measured using ultrasound, CT, or MRI and the related elastic modulus has been computed from biomechanical models of tissues. In particular, the MR elastography method (MRE) using harmonic shear waves offers direct visualization and quantitative measurement of tissue displacements, high sensitivity to very small motions, a field of view unencumbered by acoustic window requirements, and the ability to obtain full three dimensional displacement information throughout a volume [37]. The process of generating elastograms using MRI is as follows. MR images are recorded while a vibrating plate placed on the skin propagates mechanical shear waves in the tissue. By putting the magnetic field in tune with the mechanical vibrations, the wavelengths of the propagating shear waves can be calculated and used in a biomechanical model of the tissue to further calculate the corresponding Young moduli. In particular, to find the stiffness of the brain tissue, vibrations can be applied either as vertical displacements to the base of the head, or as

horizontal displacements to mouth via a bite block (Fig. 2-2.1, [19]). The Young's moduli of the white and gray matters are approximately 14.2kPa, and 5.3kPa, respectively [19]. Experimental work is underway at Penn State to estimate stiffness values of brain tumors.

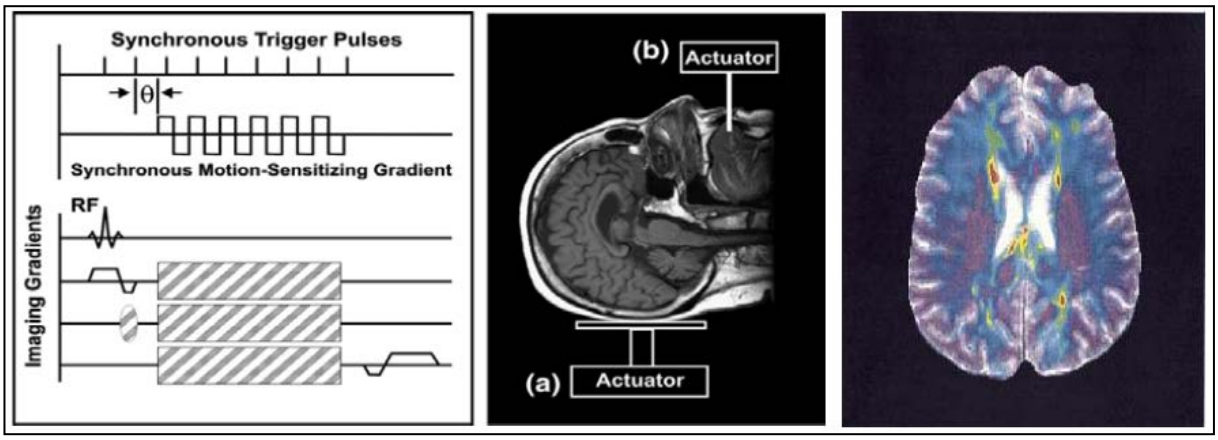

Figure 2-2.1: MRE experiment setup (left and center) and a 2D elastogram (right) [19].

2.3 Tumor Grading

Tumor grading is a system used to classify cancer cells in terms of how abnormal they look under a microscope and how quickly the tumor is likely to grow and spread. Histological grade, also called differentiation, refers to how much the tumor cells resemble normal cells of the same tissue type. Finally, nuclear grade refers to the size and shape of the nucleus in tumor cells and the percentage of tumor cells that are dividing [11].

Based on the microscopic appearance of cancer cells, pathologists commonly describe tumor grade by four degrees of severity: Grades 1, 2, 3, and 4. Cells of Grade 1 resemble normal cells, and tend to grow and multiply slowly. Grade 1 tumors are generally considered the least aggressive in behavior. However, cells of Grade 3 or Grade 4 do not look like normal cells of the same type. Grade 3 and 4 tumors tend to grow rapidly and spread faster than tumors with a lower grade. In Table 1 we show the guidelines for tumor grading recommended currently by the American Joint Commission on Cancer.

Table 1: Tumor grading [11].

Grade	Description
GX	Grade cannot be assessed (Undetermined grade)
G1	Well-differentiated (Low grade)
G2	Moderately differentiated (Intermediate grade)
G3	Poorly differentiated (High grade)
G4	Undifferentiated (High grade)

Thus, high grade tumors cannot be easily distinguished from the surrounding healthy tissue with the help of an imaging scanner. These are aggressive malignant tumors, which diffuse profusely to other parts of the body and are dangerous not only to leave them to grow in the body but also to remove them surgically. On the other hand, low grade tumors have fixed boundaries and can be well differentiated from the healthy

tissue, making their removal a safe and, in most of the cases, easy surgical procedure [12].

2.4 Review of Some Biomechanical Models for Tumors

Over the past few decades, there has been extensive progress in employing mathematical modeling to study solid tumor growth, and this work has provided insight into the understanding of experimental and clinical data. Most models fall into two categories: discrete cell-based and continuum models (see for example some recent reviews [29, 38-41]). For example, models have been applied to brain cancer [42-44] and breast cancer [45-46]. Modeling has also shown that tumor morphology may serve as a predictor of invasiveness [29, 47-50]. In [51-53], the authors revealed that cell–cell adhesion and external nutrient concentration are key parameters controlling the stability of three-dimensional multi-cellular spheroids. While Greenspan [31] considered necrotic tumors in the avascular stage, where growth is regulated solely by nutrient in the surrounding micro-environment, Byrne & Chaplain [51] proposed a model for nonnecrotic tumors where nutrient is supplied through the surrounding vascularized environment. During this avascular growth, tumor cells receive oxygen, nutrients and growth factors via diffusion through the host tissue. This phase can be investigated by *in vitro* experiments where cancer cells are cultured in a three dimensional geometry [26-29]. These experiments show that cancer cells organize into multi-cellular spheroidal colonies due to cell-cell adhesion. The outer layer of cells tends to expand and grow while the interior cells die due to the lack of nutrients. For example, the typical distance

an oxygen molecule will diffuse before being up taken is approximately 100μm. This limits the size to which a tumor spheroid can grow (1–2mm in diameter).

All the continuum models for tumors are based on reaction–diffusion equations describing the evolutions of tumor cell density, extracellular matrix (ECM), matrix-degrading enzymes (MDEs), and concentrations of cell substrates such as glucose, oxygen, and growth factors and inhibitors. For example, if we denote by Ω(t) the domain occupied by the tumor at time t, by ∑(t) the boundary between the tumor and the host tissue, ***n*** the unit outward normal vector to ∑ , and ***x*** the position vector, then the concentrations of cell substrates, such as oxygen and nutrients, σ(x,t) in Ω satisfy a reaction diffusion equation of the form:

$$\frac{d\sigma}{dt} = \nabla.(D\nabla\sigma) + \Gamma \qquad (2.4.1)$$

where *D* is the diffusion coefficient and Γ is the rate at which cell substrates are added to Ω accounting for all the sources and sinks of the substrates in the tumor volume. Usually, it is assumed that the tumor domain has constant cell density, and therefore mass changes are due to volume changes. Defining $\mathcal{V}$ to be the cells' velocity, the local rate of volume change is then given by:

$$\nabla.v = \lambda_p \qquad (2.4.2)$$

where λ_p is the net cell-proliferation rate depending on the rates of mitosis (cell division) and apoptosis (normal cell death) [32].

Different constitutive laws have been employed to describe the deformation and stress fields of the tissue. For example, the Darcy model, which models fluid flow through a porous medium, was considered in [31, 47, 51, 54], while Stokes' law of fluids was studied in [55]. Both models were investigated in [56-58]. Other continuum models have used constitutive laws for (visco-) elastic solids to predict the growth of tumors [15]. More details on such models are given in [39].

For example, if we assume that the nutrient diffusion is much faster than mitosis, then it can be shown that Darcy model reduces equation (2.4.1) to the following non-dimensional equation [32]:

$$\nabla.(\nabla\sigma) = \sigma \qquad (2.4.3)$$

If we assume that the tumor interface ∑ evolves in the direction of the normal velocity:

$$\frac{dx}{dt}.n = n.v \qquad (2.4.4)$$

then the evolution equation for the unperturbed tumor of radius r(t)=R is:

$$\frac{dR}{dt} = (1 - B)\left(\frac{1}{\tanh R} - \frac{1}{R}\right) - \frac{AR}{3} \qquad (2.4.5)$$

where the unperturbed tumor radius depends on the apoptosis parameter A, and vasculature parameter B. The right hand side is the radial component of the velocity field, which can be obtained from the Darcy constitutive law [32].

Chapter 3

Biomechanical Model based on Mass Spectra

In this chapter we propose a novel mechanical model for estimating the Young's modulus of a tissue based on its image mass spectrum.

3.1 Young's Modulus Estimation using Image Mass Spectroscopy

In order to find the Young's moduli of tumors that can be used to improve the noninvasive MRE method in the classification of tumors, we propose a novel biomechanical model based on image mass spectroscopy. Our aim is to relate the Young's modulus of a tumor to the concentration of certain proteins which have been shown to have different concentrations depending on the tumor's grade using the image mass spectroscopy approach [10]. In Fig. 3-1.1 we reproduce from [10] some image mass spectra of proteins concentrations found in low and high grade gliomas at different mass-to-charge ratios. In order to use the information provided by these images to estimate the Young's moduli of low and high grade gliomas, we make the following assumptions:

- The relative intensities of proteins given by IMS are proportional to the corresponding concentrations [20]

- The (apparent) Young's modulus of a tissue sample is proportional to the concentrations of proteins present in that tissue [13].

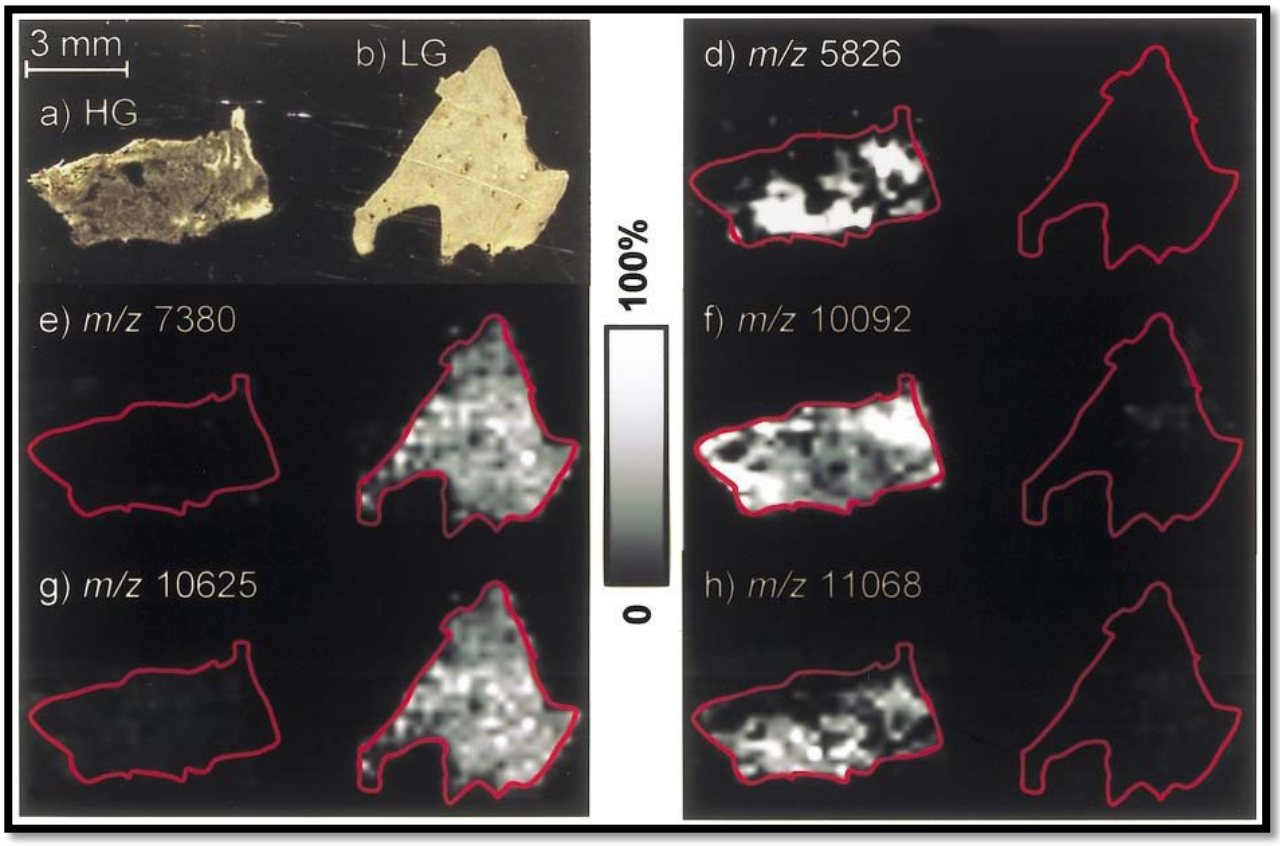

Figure 3-1.1: Ion density maps obtained at different m/z values. White represents the highest protein concentration and black represents the lowest. [10]

Figure 3-1.1 is the imaging mass spectroscopy samples of two 12 μm sections that were obtained by MALDI MS method from a low-grade tumor and a high-grade tumor human glioma biopsy. These sections were coated with a matrix using the automated spotter while the images were acquired with a lateral resolution of 250 μm [10].

In table 2 we show the averaged values of ion densities calculated from the images shown in Fig.3-1.1.

Table 2: Mean values of ion densities calculated from images shown in Fig.3-1.1.

m/z Value	Mean Value from LG Image	Mean Value from HG Image
5826	31.0676	59.6307
7380	66.4194	24.3150
10092	23.3977	73.9165
10625	70.2672	33.4180
11068	28.3134	57.4372

We propose the following expression for the apparent Young's modulus *E* dependent on the concentrations $c_n, n = 1,2, \ldots . N$ of proteins shown in Fig. 3-1.1:

$$E = \sum_{n=1}^{N} c_n^{\alpha_n\left(\frac{m}{z}\right)} \qquad (3.1.1)$$

The powers of the concentrations are assumed to depend on the corresponding mass to charge ratio (*m/z*) shown in Fig. 3-1.1 such that the apparent Young's modulus in the healthy brain tissue is approximately equal to the white matter value found by the MRE technique of 14.2 kPa [19]. We investigated the following two cases (the Matlab code is given in Appendix A):

I. $\alpha_n = 1.8 = Constant$

II. $\alpha_n = 1.6 + \frac{1}{\ln\left(\frac{m}{z}\right)_n}$

The above cases have been inspired by the results presented in [13]. Experiments on agarose gel (usually used to build phantoms that mimic the mechanical behavior of biological tissues) reported in [13] show the existence of a direct proportionality between the Young's modulus and the molar concentration of agarose. More precisely, the

Young's modulus is proportional to fractional order powers of the molar concentration. The constants of 1.8 and respectively 1.6 have been in fact proposed in [13] by fitting experimental data to a power law of concentrations for the Young's modulus. Finally, in both cases we have calibrated the coefficients such that the Young's modulus of the regions of healthy tissue is 14.2kPa as reported in the MRE literature [19].

The elastograms using formula (3.1.1) for the two cases are shown in Figs.3-1.2, 3-1.3.

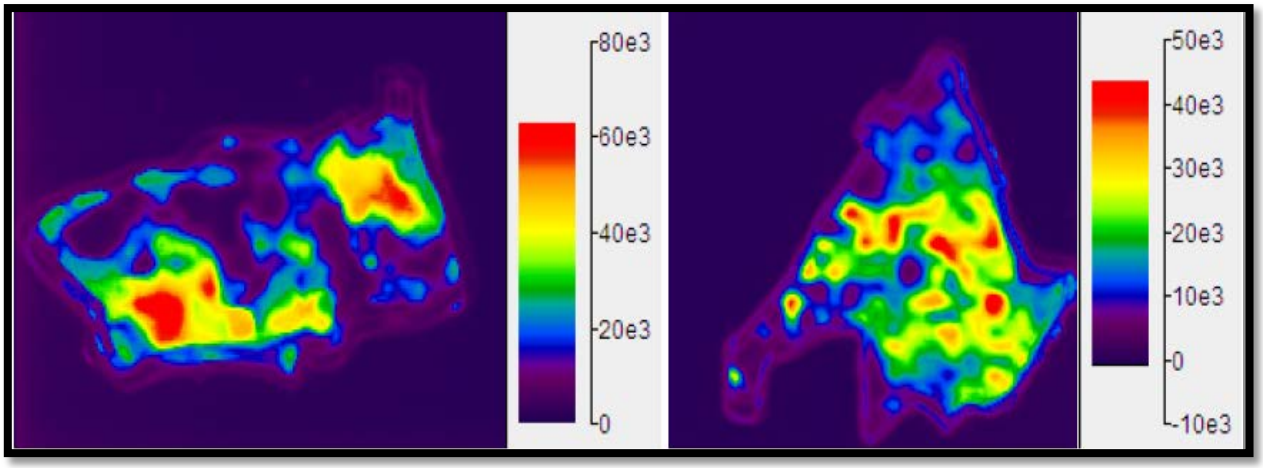

Figure 3-1.2 Elastograms of high grade (left) and low grade (right) gliomas for case I.

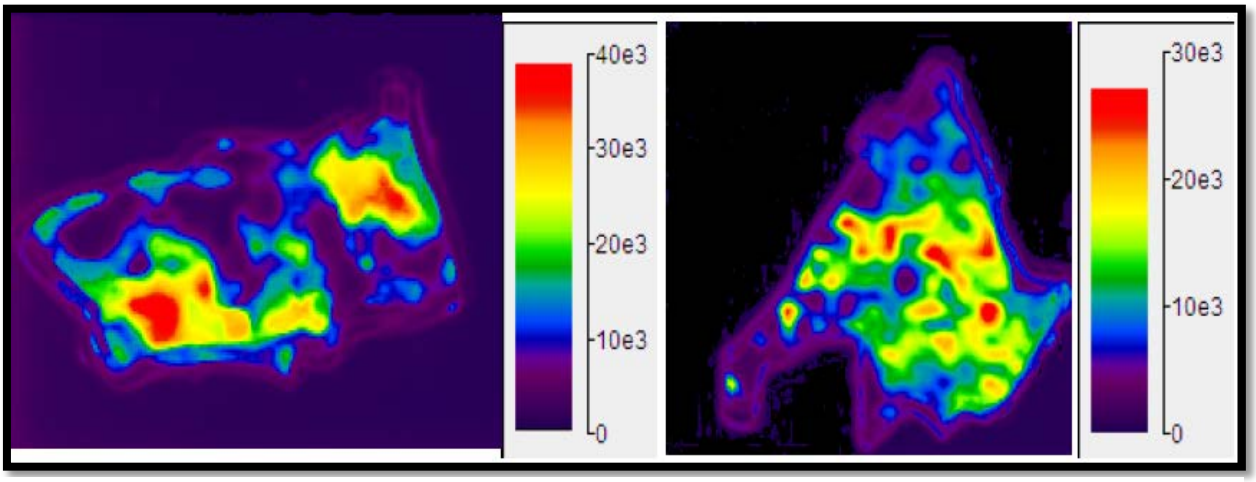

Figure 3-1.3: Elastograms of high grade (left) and low grade (right) gliomas for case II.

From Figs. 3-1.2 and 3-1.3 we conclude that *high grade gliomas are at least 10kPa stiffer than low grade gliomas. To the best of our knowledge, this is the first time when such a biomechanical model linking the stiffness of a tissue and the concentrations of proteins present in the tissue and, more importantly, when such a clear differentiation between low and high grade gliomas based on their stiffness values have been established.* These results have been published in [36].

Chapter 4

Mechano-Growth Model: Linear Case

In this chapter, we will investigate the effect of mechanics on tumor growth.

4.1 Statement of the Problem

For simplicity we will consider the case of one-dimensional growth under applied uni-axial stretch λ (Fig.4-1.1). The tumor's growth is not caused by the applied stretch, it is assumed to happen independently of the mechanics.

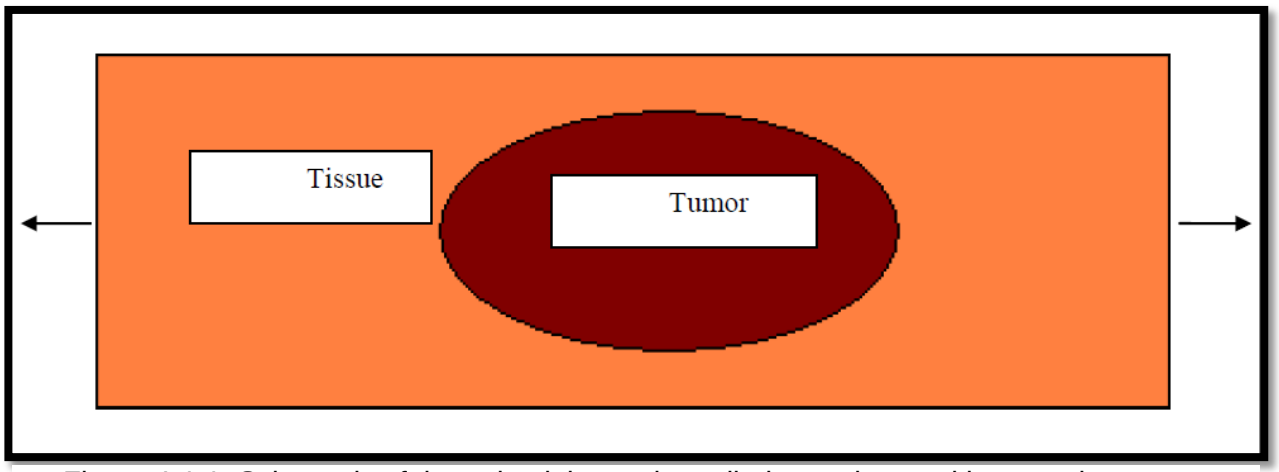

Figure 4-1.1: Schematic of the uni-axial stretch applied on a tissue with a growing tumor.

In order to make some progress in this challenging research area, we assume the growth to be volumetric and isotropic (the growth depends only on the time variable). As

in [21], a volumetric growth describes only geometric changes, the material points are dense during growth, and the intrinsic mechanical properties of the material do not change during growth. In addition, we assume for now that the tissue is an isotropic, homogeneous, linear elastic solid material.

If we denote by F_d, G, and $F = F_d G^{-1}$ the deformation gradient of the applied uni-axial stretch, the growth tensor, and, respectively, the total deformation gradient (Fig. 4-1.2), then the Cauchy stress tensor is given by Hooke's law:

$$\sigma = E\left(\frac{\lambda}{g(t)} - 1\right) \qquad (4.1.1)$$

where *E* is the Young's modulus and *g(t)* is the isotropic growth function.

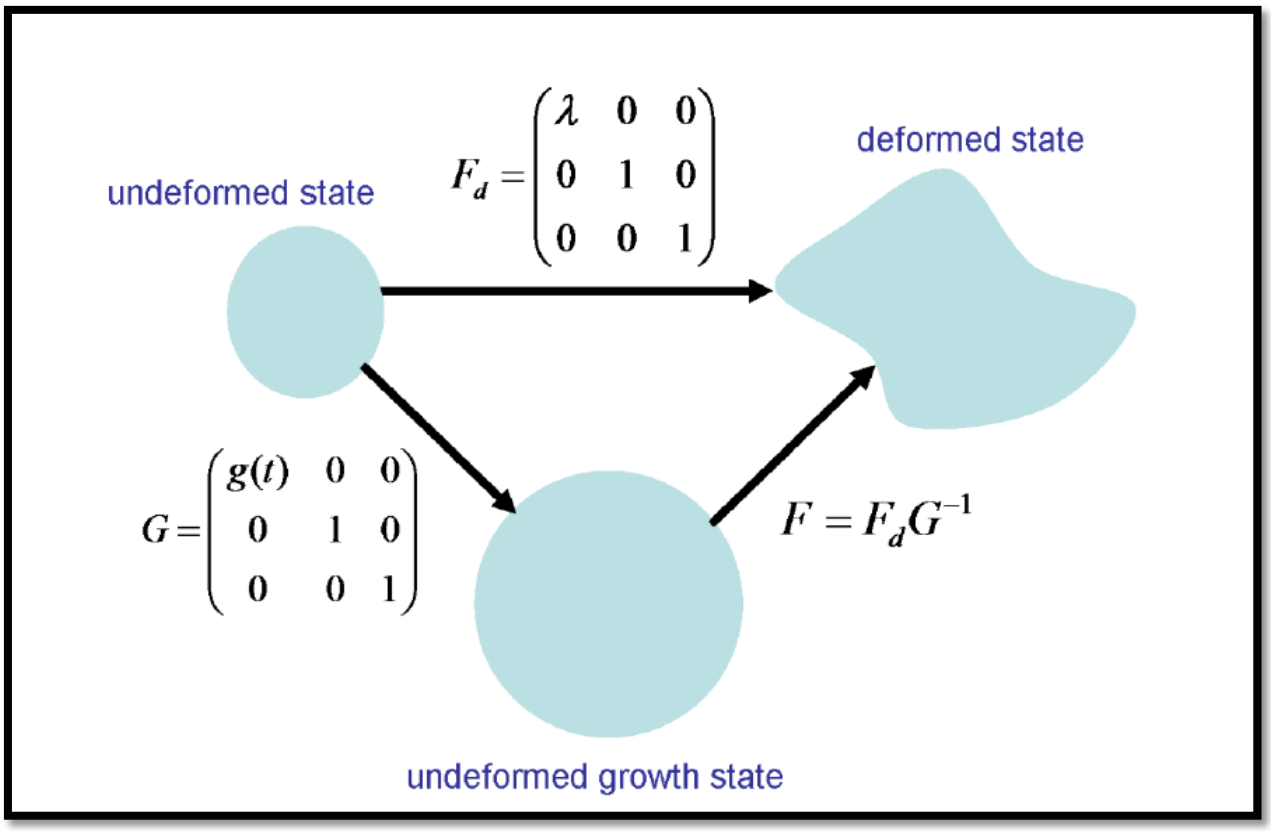

Figure 4-1.2: Kinematics of the coupled growth-deformation of a tumor.

If we replace the above expression of the stress in the equation of growth proposed in [14] (the equation is obtained from assumptions regarding the growth of viscoelastic cytoskeletal networks), we obtain the following first order, nonlinear differential equation:

$$\frac{dg(t)}{dt} = K \exp\left(\frac{\gamma E\left(\frac{\lambda}{g(t)}-1\right)}{k_B T}\right) g(t) \qquad (4.1.2)$$

where $T,\ k_B,\ \gamma$ are the absolute temperature, Boltzman constant, and a parameter depending on the bio-chemical reactions involved in the growth process, respectively. The constant parameter *K* has units of s^{-1} and is found experimentally [14]. Since we do not have experimental data, we assume for simplicity that $K = 1s^{-1}$ and omit this parameter from our further calculations.

We will like to notice here that the model proposed in [14] is simpler than the models we presented in our literature review (chapter 2). The atomistic models of tumor growth consider only diffusion and reaction of chemical species, without accounting for mechanical behavior of the tumor due to cellular mechano-transduction processes. On the other hand, the continuum models of solid tumors are computationally very demanding: they involve solving a system of coupled hyperbolic and parabolic partial differential equations that account for both, mechanics and diffusion-reaction processes. In contrast, the model proposed in [14] is a somehow simpler continuum model that has the following advantages: (1) incorporates small incremental growth and deformation,

which converts an intrinsically nonlinear problem into a linear one with cumulative elastic quantities; (2) the deformation decomposition is developed for viscoelastic media which is applicable to the cytoskeletal network, and (3) the development allows for coupling of any physically relevant phenomena such as the local stress in the material or local G-actin concentration with the growth tensor. From a computational point of view, this model requires to solve only one differential equation.

In particular, if the solid is assumed to be linear elastic with a volumetric growth and the problem is considered one-dimensional, the model proposed in [13] reduces to equation (4.1.2). This is a non-linear first order differential equation that we will solve analytically in the next chapter. For the beginning, we consider the linearized form of equation (4.1.2). The initial condition used in all of the numerical simulations is: $g(0) = 1.$

4.2 The Classic Linear Case

The linearized form of equation (4.1.2) is:

$$\frac{d(\ln(g(t))}{dt} = \exp\left(\frac{\gamma E(\lambda-1)}{k_B T}\right)\left(1 - \frac{\gamma E\lambda}{k_B T}\ln(g(t))\right) \qquad (4.2.1)$$

with the solution given by:

$$g(t) = \exp\left(\frac{\exp\left(\frac{\gamma E(\lambda-1)}{k_B T}\right)}{\frac{\gamma E \lambda}{k_B T}} \left(1 - \exp\left(-\exp\left(\frac{\gamma E(\lambda-1)}{k_B T}\right)\frac{\gamma E \lambda}{k_B T} t\right)\right)\right) \quad (4.2.2)$$

Solution (4.2.2) is represented in Fig.4-2.1 for different values of the stretch λ for low and high grade gliomas (the Matlab code used to generate these plots is given in Appendix A). We use the following known physical parameters [14]:

$$\gamma = 1.3\times 10^{-26}\,\mathrm{m}^3,\ k_B = 1.3\times 10^{-23}\,\mathrm{m}^2\times \mathrm{Kg}/(\mathrm{s}^2\times \mathrm{K}),\ T = 298\mathrm{K}$$

We plot the growth function $g(t)$ as given by formula (4.2.2) for a low grade glioma of averaged stiffness $E_{low} = 35\mathrm{kPa}$ and for a high grade glioma of averaged Young's modulus $E_{high} = 50\mathrm{kPa}$. These averaged stiffness values were estimated from Figs. 3-1.2 and 3-1.3.

We note that for small stretches 0 < λ ≤1 the growth of a low grade glioma appears to be as fast as that of a high grade glioma. However, as the stretch increases and we approach the limits of validity of the linearity assumption for the tissue, the low grade glioma increases much faster than the high grade glioma and both types of tumors will reach limiting sizes after which they will stop growing. These sizes are determined by the applied stretch.

However, it is expected that our assumption of a linear elastic tumor will limit the applicability of the growth function (4.2.2) for large but finite stretches, so the behavior seen in Fig. 4-2.1 when λ = 10, is most likely unphysical.

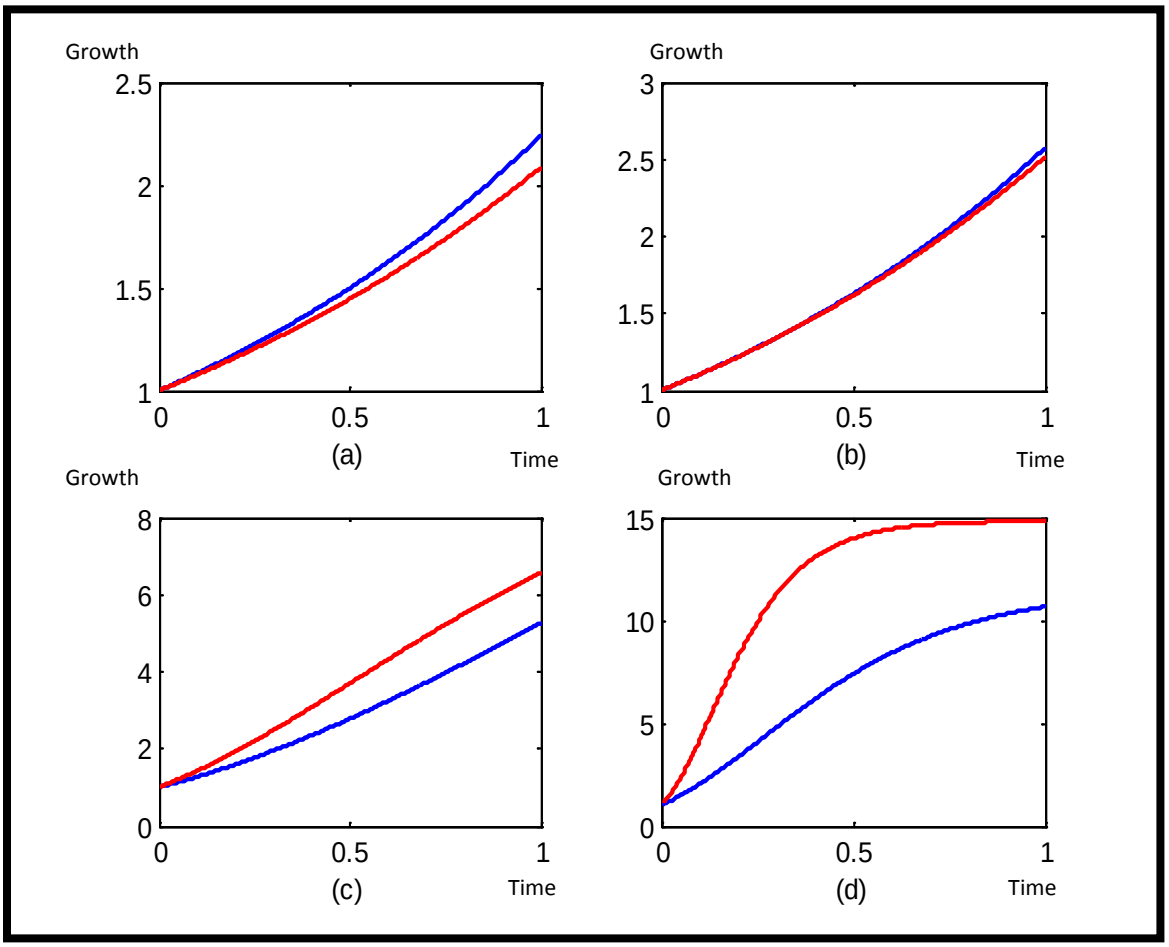

Figure 4-2.1: Growth functions given by formula (4.2.2) of low grade (blue) and high grade (red) glioma versus a normalized time scale for (a) λ =0.1, (b) λ =1, (c) λ =5, and (d) λ =10.

4.3 The Fractional Order Linear Case

We replace now the first order temporal derivative in equation (4.2.1) by the left sided Riemann-Liouville fractional order derivative and we obtain the following growth equation:

$$D^{\alpha}(\ln(g(t)) = \exp\left(\frac{\gamma E(\lambda-1)}{k_B T}\right)\left(1 - \frac{\gamma E\lambda}{k_B T}\ln(g(t))\right) \qquad (4.3.1)$$

By definition, the left-sided Riemann-Liouville fractional order derivative of order $\alpha \in (0, 1]$ of a function $f \in L^1([0, \infty))$ is:

$$D^{\alpha} f(t) = \begin{cases} \frac{1}{\Gamma(1-\alpha)} \frac{d}{dt} \int_0^t \frac{f(s)ds}{(t-s)^{\alpha}}, \alpha \epsilon (0,1) \\ \frac{d}{dt} f(t), \alpha = 1 \end{cases}$$

where $\Gamma(s) = \int_0^{\infty} e^{-t} t^{s-1} dt$ is the gamma function. Note that equation (4.2.1) is a particular case of equation (4.3.1) for $\alpha = 1$. Lately, fractional order derivative models have been used in a wide range of engineering and science problems such as signal and image processing, economics, control theory, dynamical systems, pattern recognition, viscoelastic behaviors of materials (especially polymers and biological tissues like lung and brain).

We apply the Laplace transformation method to solve equation (4.3.1). If we denote by $L(f(t))$ the Laplace transform of f and use the fact that:

$$\mathrm{L}\left(\mathrm{D}^{\alpha}\mathrm{f}(\mathrm{t})\right) = \mathrm{s}^{\alpha}\mathrm{L}\left(\mathrm{f}(\mathrm{t})\right),\ \ \mathrm{L}^{-1}\left(1/\mathrm{s}^{1-\alpha\mathrm{k}}\right) = \frac{\mathrm{t}^{-\alpha\mathrm{k}}}{\Gamma(1-\alpha\mathrm{k})},$$

we obtain (after a few simple algebraic manipulations):

$$g(t) = \exp\left(\sum_{k=0}^{\infty} \frac{(-1)^k}{\left(\exp\left(\frac{\gamma E(\lambda-1)}{k_B T}\right)\right)^k \left(\frac{\gamma E\lambda}{k_B T}\right)^{k+1}} \frac{t^{-\alpha k}}{\Gamma(1-\alpha k)}\right) \quad (4.3.2)$$

We use the same values for the physical parameters as in section 4.2 to plot the growth function given by formula (4.3.2) for a uni-axial stretch value of λ=10 and different values of fractional order α (see Fig. 4-3.1).

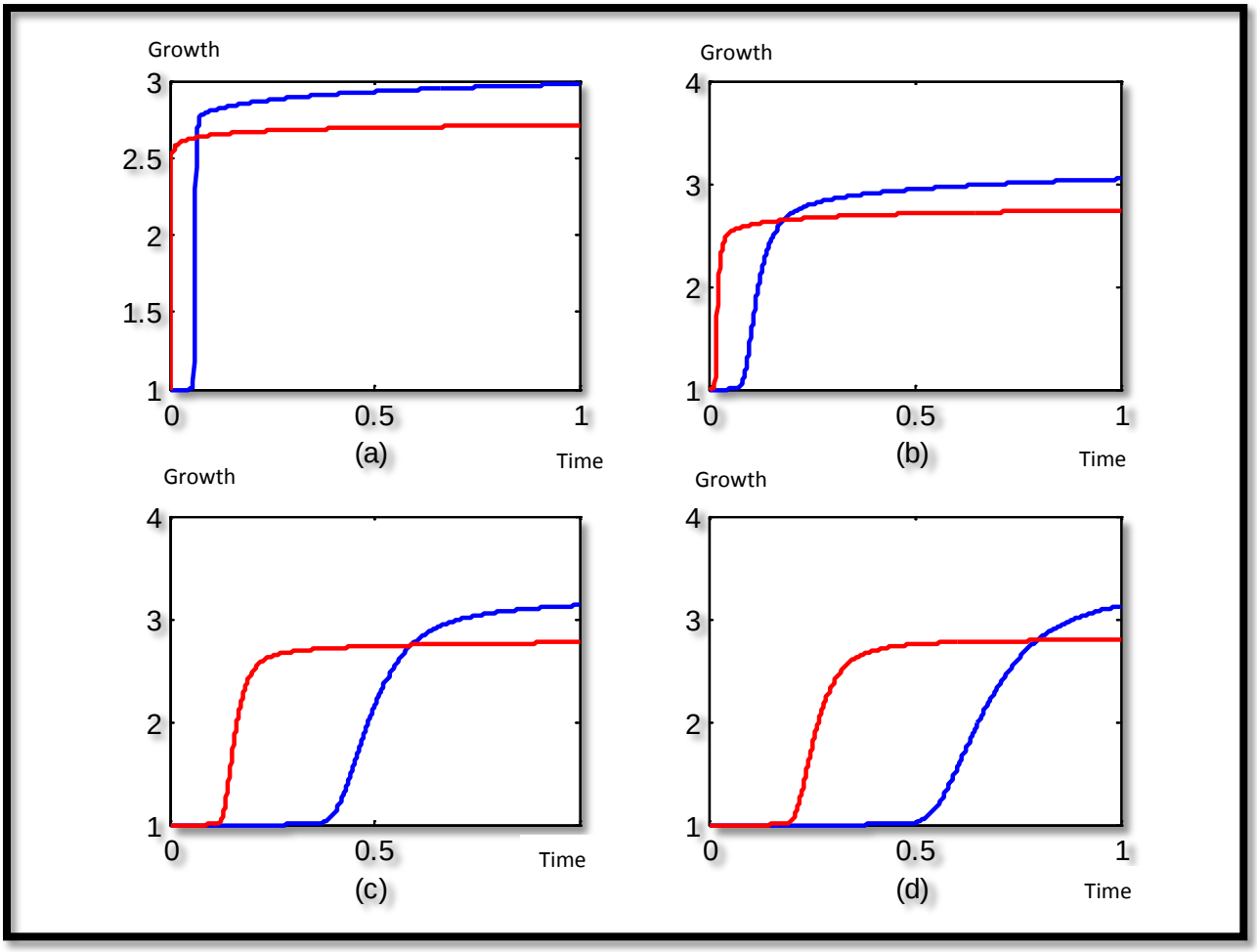

Figure 4-3.1: Growth functions given by formula (4.3.2) of low grade (blue) and high grade (red) glioma versus a normalized time scale for λ = 10 and: a) α = 0.25; b) α = 0.5; c) α = 0.75; d) α = 0.9.

Using formula (4.3.2) we noticed that for small values of applied stretch λ (but not very small since the series given by (4.3.2) diverges in these cases) and for values of α between 0 and 1, the growth remains constant for both types of gliomas. However, as the stretch becomes large but finite, the growth functions of low grade and high grade gliomas not only increase with time but also show that at a certain moment**,** *a low grade glioma can grow faster than a high grade glioma signaling its transformation into cancer.* As it can be seen in Fig. 4-3.1, as α increases, not only that the very sharp growth of both low and high grade gliomas starts later, but also the time when the low grade

becomes a high grade tumor is delayed. Also, since the growth behavior shown in Fig. 4-3.1 is noticed for a relatively large stretch (approximately $\lambda > 5$) where the linear elasticity assumption might not be valid anymore, we believe that the fractional order temporal derivative could account for some of the microscopic heterogeneity and material nonlinearities which are not captured by the macroscopic Hooke's law. In materials with evolving microstructure the fractional order α might connect not only multiple time scales but also time *and* length scales. We believe that our fractional order mechano-growth model incorporates an inhomogeneous clock that connects the macroscopic global and the microscopic local time (*and possibly length*) scales through the presence of a fractional order temporal derivative. In this form, the model is able to predict the time when a low grade tumor transforms into cancer at large but finite stretches. The results presented in this chapter have been published in [36].

Chapter 5

Mechano-Growth Model: Non-Linear Case

In this chapter we turn our attention to solving the original non-linear differential equation we proposed in the previous chapter as our mechano-growth model. We will use the Adomian decomposition method to find analytical solutions to both – the classic first order and the corresponding generalized fractional order – nonlinear differential equations.

5.1 Brief Review of the Adomian Decomposition Method

Almost thirty years ago, Adomian proposed a new decomposition method to obtain analytical solutions to a wide class of both deterministic and stochastic ordinary and partial differential equations "*without linearization or weak nonlinearity assumptions, closure approximations, perturbation theory, or restrictive assumptions on stochasticity*" [35]. In many recent publications dealing with solutions to nonlinear partial differential equations, the Adomian method proved to be as fast and as accurate as numerical methods usually used to solve differential equations such as the finite element method (see, for instance, [60]) .

In what follows we will present the main steps of the Adomian method used in solving an equation of the form: $Fu(t) = g(t)$, where F represents a general nonlinear ordinary

differential operator involving both linear and nonlinear terms. The linear term is decomposed into $L + R$, where L is easily invertible and R is the remainder of the linear operator. For convenience, L is usually taken to be the highest order derivative which avoids difficult integrations which result when complicated Green's functions are involved. Thus the equation may be written as [35]:

$$Lu + Ru + Nu = g \tag{5.1.1}$$

where Nu represents the nonlinear term. Since the linear operator L is invertible, equation (5.1.1) can be re-written as:

$$L^{-1}Lu = L^{-1}g + L^{-1}Ru - L^{-1}Nu \tag{5.1.2}$$

If this corresponds to an initial-value problem, the integral operator L^{-1} may be a definite integral. If L is a second-order operator, L^{-1} is a twofold integration operator and $L^{-1}Lu = u - u(t_0) - (t - t_0)\,u'(t_0)$. Solving equation (5.1.2) gives [35]:

$$u = A + Bt + L^{-1}g - L^{-1}Ru - L^{-1}Nu \tag{5.1.3}$$

We assume now that the following decomposition of the nonlinear term Nu is valid:

$$Nu = \sum_{n=0}^{\infty} A_n, \tag{5.1.4}$$

where A_n are special polynomials of the following form:

$$A_0 = f(u_0)$$

$$A_1 = u_1 \left(\frac{d}{du_0}\right) f(u_0)$$

$$A_2 = u_2 \left(\frac{d}{du_0}\right) f(u_0) + \left(\frac{u_1^2}{2!}\right)\left(\frac{d^2}{du_0^2}\right) f(u_0)$$

were, as in [35], we denote by *Nu=f(u).*

Then the analytic solution (5.1.3) can be written as a series solution of the form $\sum_{n=0}^{\infty} u_n$, with $u_0=A+Bt+L^{-1}g$ and:

$$\sum_{n=0}^{\infty} u_n = u_0 - L^{-1}R\sum_{n=0}^{\infty} u_n - L^{-1}\sum_{n=0}^{\infty} A_n \qquad (5.1.5)$$

From (5.1.5) it follows that:

$$u_1 = -L^{-1}Ru_o - L^{-1}A_0 \qquad (5.1.6)$$

$$u_2 = -L^{-1}Ru_1 - L^{-1}A_1$$

$$\dots$$

$$u_{n+1} = -L^{-1}Ru_n - L^{-1}A_n$$

It has been shown that the Adomian method series solution $u = \sum_{n=0}^{\infty} u_n$, where $u_n, n = 0,1, \ldots$ are given by formulas (5.1.6), converges relatively fast to the exact solution of equation (5.1.1) [35].

5.2 The Classic Non-Linear Case

We consider again equation (4.1.2) for $K = 1s^{-1}$, namely:

$$\frac{dg(t)}{dt} = \exp\left(\frac{\gamma E\left(\frac{\lambda}{g(t)} - 1\right)}{k_B T}\right) g(t) \qquad (5.2.1)$$

We used Mathematica to solve this equation using the Adomian decomposition method (the code can be found in Appendix A). The physical parameters used with the Adomian method are given in Table 3 (the average Young's modulus values for low (E_{low}) and high (E_{high}) grade gliomas are taken from chapter 2).

Table 3: Physical parameters used with the Adomian method.

Parameter	Value
γ	1.3×10^{-26} m^3
k_B	1.3×10^{-23} m^2*Kg/(s^2*K)
T	298 K
E_{low}	$30 \times 10^3 Pa$
E_{high}	$40 \times 10^3 Pa$
g_0	1

The Adomian method series solution converges to the exact solution of equation (5.2.1) in only 4 terms:

$$\mathrm{g(t)} = \mathrm{g}_0 + e^{\frac{\gamma\left(-1+\frac{\lambda}{\mathrm{g}_0}\right)\mathrm{E}}{k_B T}}\mathrm{g}_0 t + \frac{e^{\frac{2\gamma\left(-1+\frac{\lambda}{\mathrm{g}_0}\right)\mathrm{E}}{k_B T}} t^2 (k_B \mathrm{g}_0 T - \gamma\lambda\mathrm{E})}{2k_B T} + \frac{e^{\frac{3\gamma\left(-1+\frac{\lambda}{\mathrm{g}_0}\right)\mathrm{E}}{k_B T}} t^3 \left(k_B{}^2 \mathrm{g}_0{}^2 T^2 - 2\gamma k_B \lambda \mathrm{g}_0 T\mathrm{E} + 2\gamma^2\lambda^2\mathrm{E}^2\right)}{6k_B{}^2 \mathrm{g}_0 T^2} + \frac{e^{\frac{4\gamma\left(-1+\frac{\lambda}{\mathrm{g}_0}\right)\mathrm{E}}{k_B T}} t^4 \left(k_B{}^3 \mathrm{g}_0{}^3 T^3 - 3\gamma k_B{}^2 \lambda \mathrm{g}_0{}^2 T^2 \mathrm{E} + 4\gamma^2 k_B \lambda^2 \mathrm{g}_0 T\mathrm{E}^2 - 6\gamma^3\lambda^3\mathrm{E}^3\right)}{24k_B{}^3 \mathrm{g}_0{}^2 T^3} \quad (5.2.2)$$

By replacing the values of the Young's modulus *E* in equation (5.2.2) by the values of E_{low} and E_{high} given in Table 3, we plot the growth functions for low and high grade gliomas against time for various stretch values λ as shown in Figs.5-2.1, 5-2.2, 5-2.3 and respectively 5-2.4.

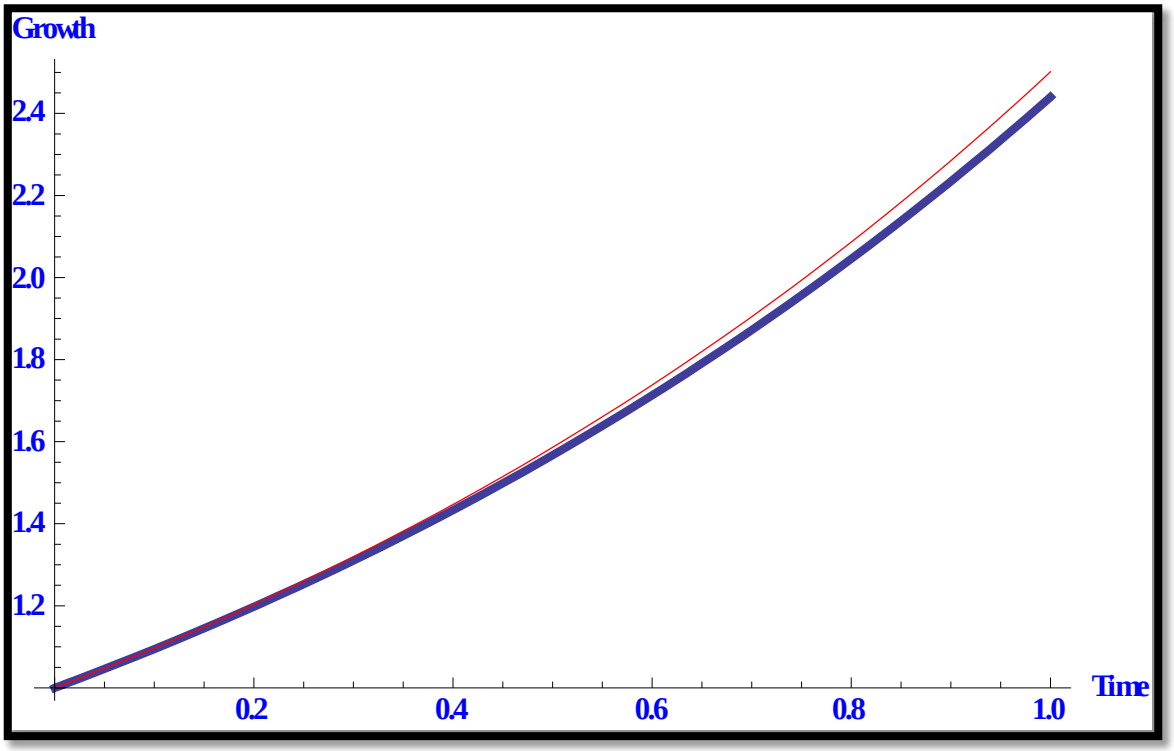

Figure 5-2.1: Growth functions given by formula (5.2.2) of high-grade (red) and low grade (blue) gliomas versus a normalized time scale for λ=0.25.

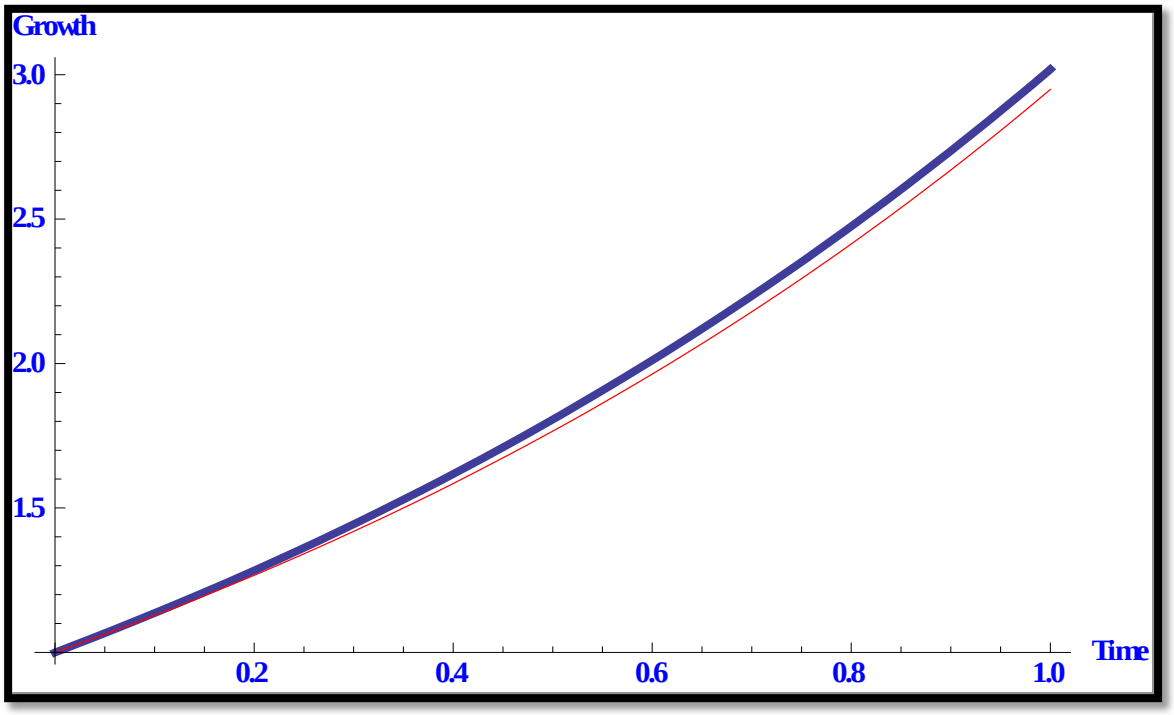

Figure 5-2.2: Growth functions given by formula (5.2.2) of high-grade (red) and low grade (blue) gliomas versus a normalized time scale for λ=3.

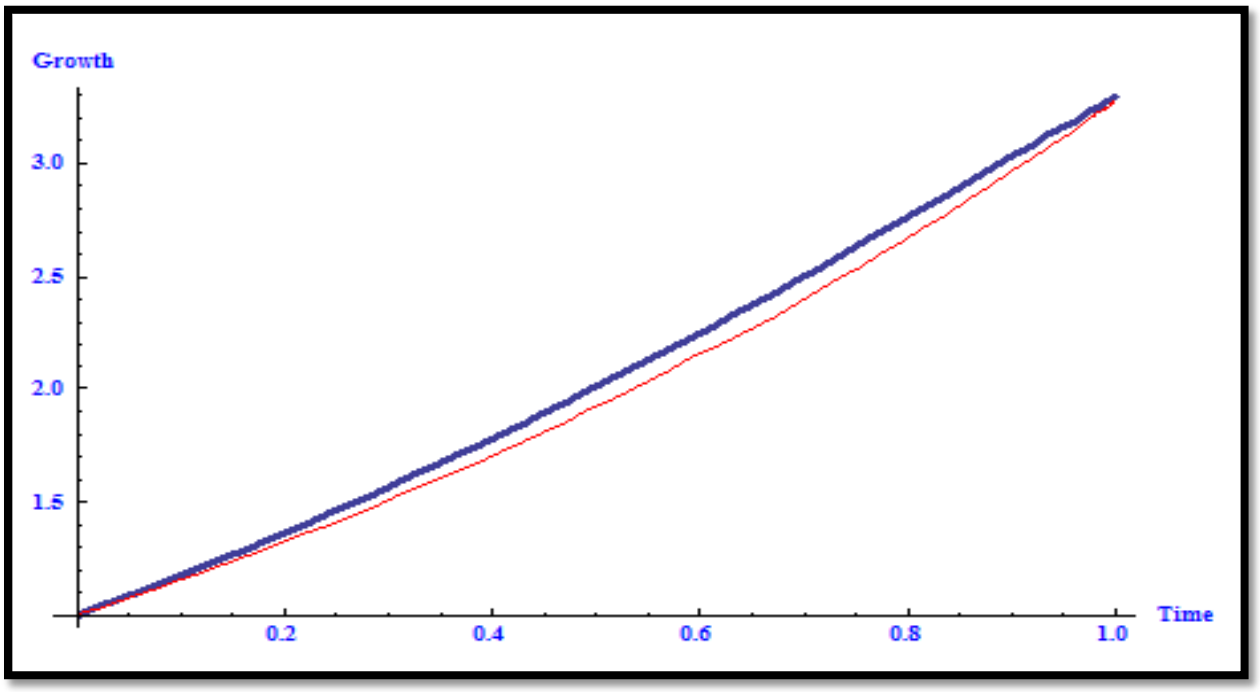

Figure 5-2.3: Growth functions given by formula (5.2.2) of high-grade (red) and low grade (blue) gliomas versus a normalized time scale for λ=5.

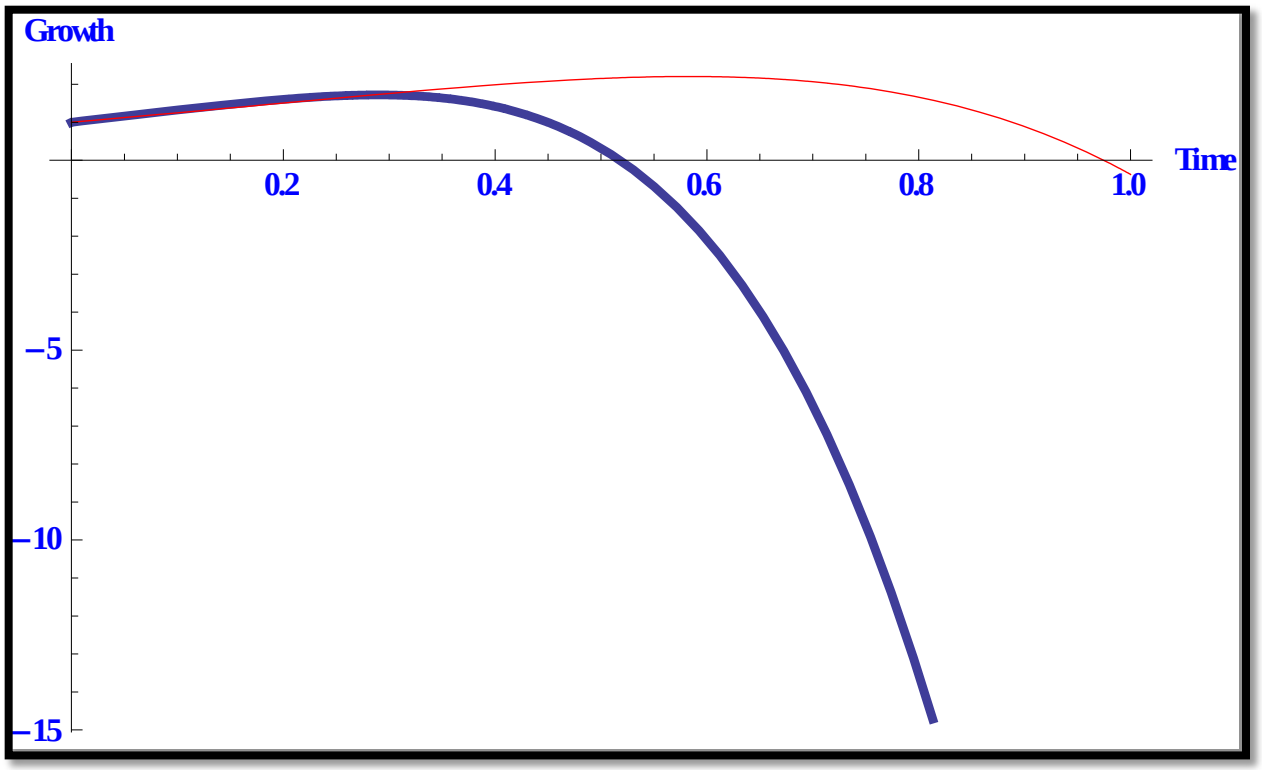

Figure 5-2.2: Growth functions given by formula (5.2.2) of high-grade (red) and low grade (blue) gliomas versus a normalized time scale for λ=10.

From these graphs we can see that at low stretches λ the high-grade gliomas grow more aggressively than the low-grade gliomas (Fig.5-2.1), while as the stretch increases, the low-grade gliomas grow a little bit more than the high-grade gliomas (Figs. 5-2.2 and 5-2.3). At large but finite stretches the linearity of the material no longer holds true, so equation (5.2.1) is not valid anymore and its solution (5.2.2) becomes unphysical (Fig.5-2.4).

5.3 The Fractional-Order Non-Linear Case

We consider now the corresponding generalized fractional order differential equation to equation (5.2.1):

$$D^{\alpha} g(t) = \exp\left(\frac{\gamma E\left(\frac{\lambda}{g(t)} - 1\right)}{k_B T}\right) g(t) \qquad (5.3.1)$$

The Adomian decomposition method can be applied again to solve equation (5.3.1). As in [61], we apply first the inverse (integral) operator $\boldsymbol{D^{-\alpha}}$ to equation (5.3.1) and then follow the same steps as in the classic Adomian method. The terms in the Adomian method series solution to equation (5.3.1) have been again computed using Mathematica and given the length and complexity of these terms we will not reproduce it here.

In our numerical simulations we used λ=0.25, and λ = 5, and for each λ value, three different α values were considered: α=0.25, α=0.5, and α=0.9. The results are shown in Figs.5-3.1, 5-3.2, 5-3.3 for λ=0.25, and in Figs. 5-3.4, 5-3.5, 5-3.6 for λ=5.

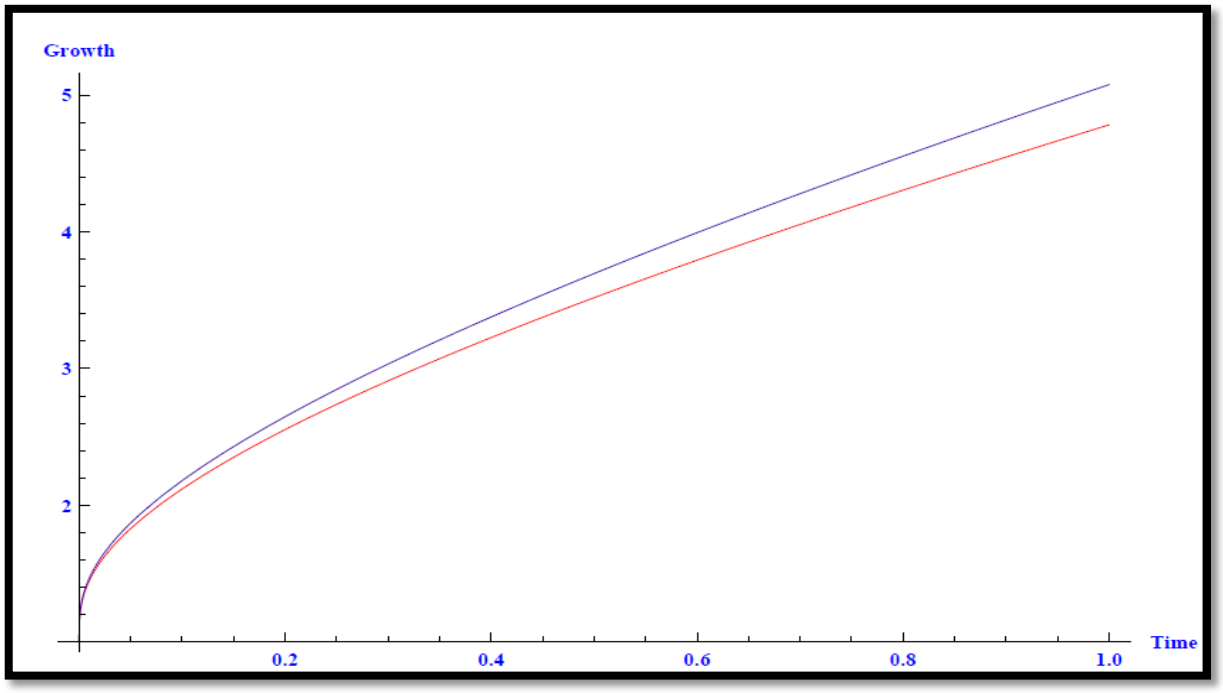

Figure 5-3.1: Growth functions for high-grade (red) and low grade (blue) gliomas versus a normalized time scale for for λ=0.25 and α = 0.25.

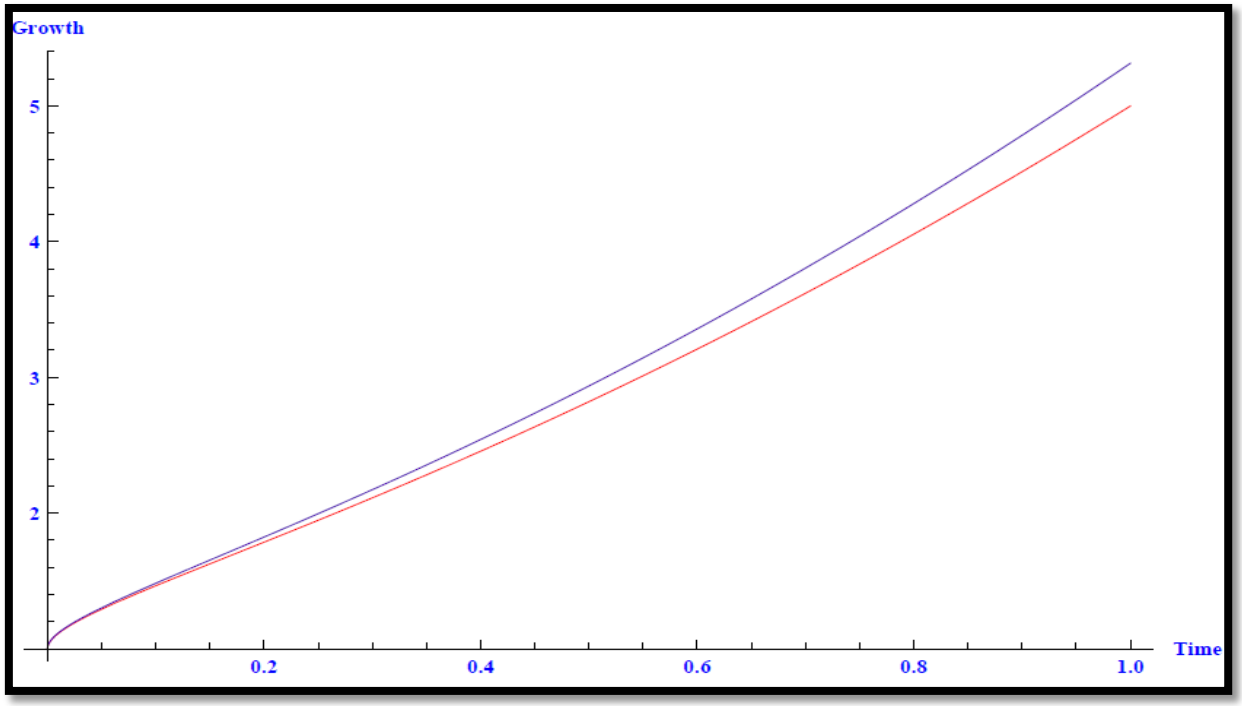

Figure 5-3.2: Growth functions for high-grade (red) and low grade (blue) gliomas versus a normalized time scale for for λ=0.25 and α = 0.5.

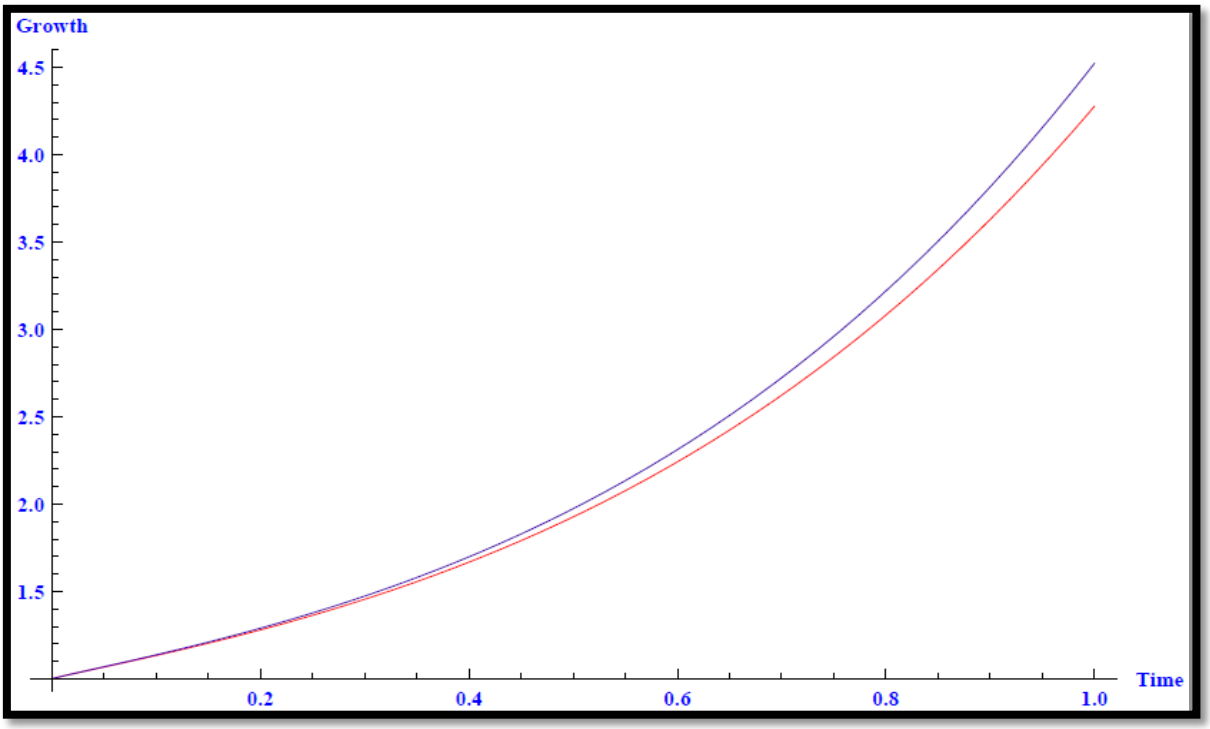

Figure 5-3.3: Growth functions for high-grade (red) and low grade (blue) gliomas versus a normalized time scale for for λ=0.25 and α = 0.9.

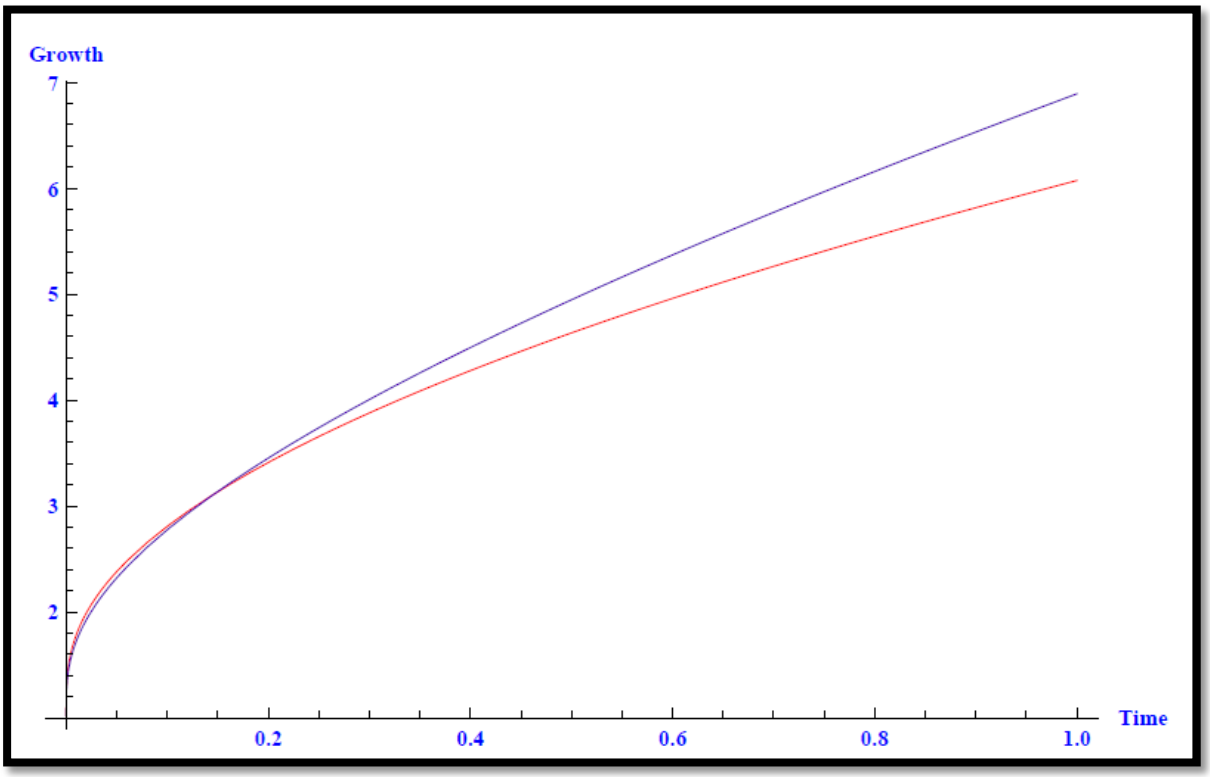

Figure 5-3.4: Growth functions for high-grade (red) and low grade (blue) gliomas versus a normalized time scale for for λ=5 and α = 0.25.

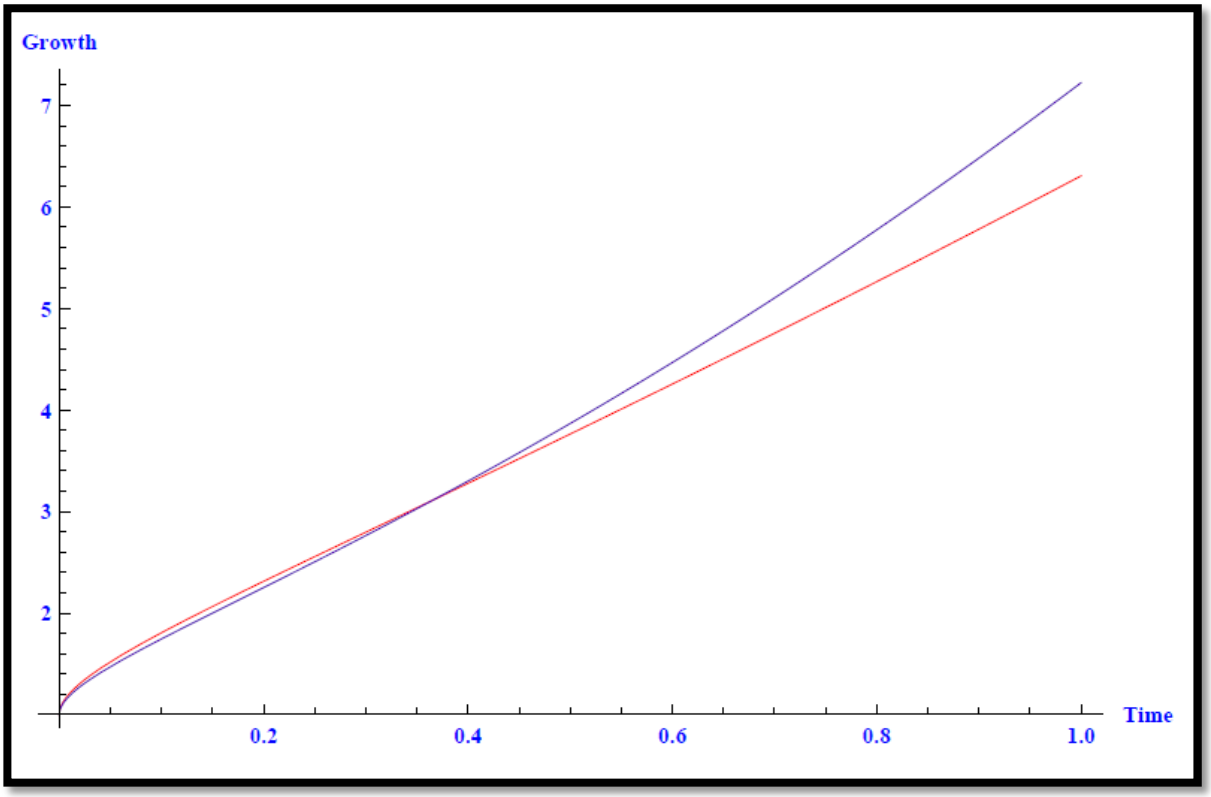

Figure 5-3.5: Growth functions for high-grade (red) and low grade (blue) gliomas versus a normalized time scale for for λ=5 and α = 0.5.

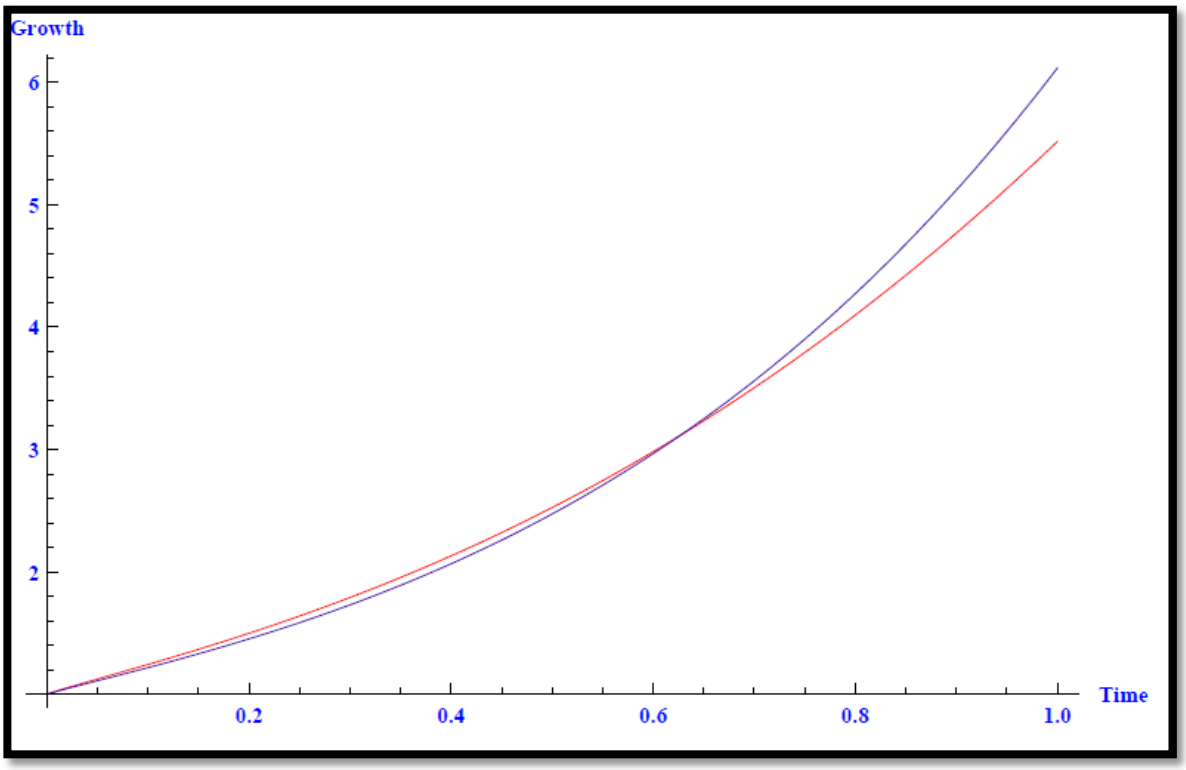

Figure 5-3.6: Growth functions for high-grade (red) and low grade (blue) gliomas versus a normalized time scale for for λ=5 and α = 0.9.

From these graphs we see again as in the linearized case that for larger stretch values λ the growth of a low grade glioma can become larger than the growth of a high grade glioma. Unlike the linearized case, we were able to find convergent Adomian series for small stretch values and every value of the fractional order α. We also notice that for a fixed stretch value, the convexity of the growth functions changes with increasing α (the curve is concave for $\alpha<0.5$, and it becomes convex for $\alpha>0.5$). Such information could be of crucial importance for treatment decisions and planning. Finally, by comparing Figs.5-3 for the fractional order model and Figs.5-2 for the classic model we see that the trend noticed in the linearized case is maintained: the classic case does not capture the transition of a tumor from low grade to high grade.

Chapter 6

Conclusion and Future Work

In this thesis we proposed two novel biomechanical models: one that estimates the Young's moduli of low and high grade tumors (we considered here only gliomas) based on the concentrations of proteins as given by image mass spectroscopy, and another model that predicts the growth behavior of these two types of brain tumors under uni-axial stretch. Our first model showed that we can differentiate between low and high grade gliomas based on their (apparent) stiffness, a high grade being at least 10kPa stiffer than a low grade glioma. Such information can play an important role in the development of better, non-invasive diagnostic and treatment planning procedures based on image elastography. The next step will be to validate this model experimentally on tumors from different types of tissues.

Our mechano-growth model showed how an applied uni-axial stretch λ can affect the growth of low and high grade gliomas. For simplicity we assumed that the tissue is an isotropic homogeneous linear elastic solid for which the stress-strain relationship is given by Hooke's law and that tumor growth is regulated by the growth of the viscoelastic cytoskeletal networks present in the tissue. This assumptions lead to a non-linear first order evolution equation similar to the one proposed in [14]. We generalized this equation by replacing the first order temporal derivative by a fractional order one. We have shown that by using a fractional order temporal derivative instead of a first

order one, we can predict when a low grade glioma becomes a high grade (cancerous) tumor. While the idea of using fractional order temporal derivatives to describe abnormal processes believed to be involved in the birth of tumors is not new (see, for example, [59]), our study on the effect of the fractional derivative on the coupling between the growth and biomechanics of tumors is, to the best of our knowledge, novel. Living biological materials are dynamic materials whose microstructure is evolving continuously. The fractional order α can be seen as modeling an inhomogeneous clock that connects the macroscopic global time scale and the microscopic local time and length scales. We have solved first the linearized equations and then we used the Adomian decomposition method to find analytical solutions to both the classic and the generalized fractional order non-linear evolution equations. While the classic model predicts that the high grade tumors grow somehow faster than the low grade ones, the fractional order model captures the transition of a low grade tumor to a high grade one regardless of the amount of mechanical stretch applied. Also, the size of the fractional order α appears to play an important role in this growth process: the shape of the growth curve changes from concave to convex as α increases. This piece of information could prove crucial in treatment decisions and planning. In our further work we plan to investigate how this fractional order relates to bio-chemical processes (described by diffusion-reaction differential equations) taken place in tissues and tumors. A multi-scale approach might have to be considered.

References

1. Aebersold, R., Goodlett, D. R. (2001). Mass spectrometry in proteomics. *Chem. Rev.* 101: 269–95.
2. Russell, D. H., Edmondson, R. D. (1997). High-resolution mass spectrometry and accurate mass measurements with emphasis on the characterization of peptides and proteins by matrix-assisted laser desorption/ionization time-of-flight mass spectrometry. *J. Mass Spectrom.* 32: 263–76.
3. Cotter, R. J. (1999). The new time-of-flight mass spectrometry. *Anal. Chem.* 71: 445A–51A.
4. Todd, P. J., Schhaaff, T. G., Chaurand, P., Caprioli, R. M. (2001). Organic ion imaging of biological tissue with SIMS and MALDI. *J. Mass Spectrom.* 36: 355–69.
5. Chaurand, P., Caprioli, R. M. (2002). Direct profiling and imaging of peptides and proteins from mammalian cells and tissue sections by mass spectrometry. *Electrophoresis* 23: 3125–35.
6. Chaurand, P., Schwartz, S. A., Caprioli, R. M. (2002). Imaging mass spectrometry: a new tool to investigate the spatial organization of peptides and proteins in mammalian tissue sections. *Curr. Opin. Chem. Biol.* 6: 676–81.
7. Chaurand, P., Schwartz, S. A., Caprioli, R. M. (2004). Profiling and imaging proteins in tissue sections by mass spectrometry. *Anal. Chem.* 76: 86A–93A.
8. Quong, J. N., Knize, M. G., Kulp, K. S., Wu, K. J., (2004). Molecule specific imaging analysis of carcinogens in breast cancer cells using time-of-flight secondary ion mass spectrometry. *Appl. Surface Sci.* 231: 424–427.
9. Schwartz, S. A., Reyzer, M. L., Caprioli, R. M. (2003). Direct tissue analysis using matrix-assisted laser desorption/ionization mass spectrometry: practical aspects of sample preparation. *J. Mass Spectrom.* 38: 699–708.
10. Chaurand P., Schwartz S., Reyzer M., Caprioli R. (2005). Imaging mass spectroscopy: principles and potentials. *Toxicologic Pathology* 33: 92-101.
11. Tumor Grade: Q&A - National Cancer Institute. http://www.cancer.gov/cancertopics/factsheet/Detection/tumor-grade
12. Tumor - Body, Process, Type, Characteristics, Cells, Surface, Part, Benign and Malignant Tumors, Medical Approaches. http://www.scienceclarified.com/Ti-Vi/Tumor.html
13. Normand V., Lootens D.L., Amici E., Plucknett K.P., Aymard P. (2000). New insight into agarose gel mechanical properties. *Biomacromolecules*, *American Chemical Society* 1, 730–738.
14. Kim J.S., Sun S.X. (2009). Continuum modeling of forces in growing viscoelastic cytoskeletal networks. *J.Theor. Biol.* 256: 596-606.
15. Oliver C., Sermesant M., Bondiau P.Y., Delingette H., Warfield S., Malandain G., Ayache N. (2005). Realistic simulation of the 3D growth of brain tumors in MR images coupling diffusion with biomechanical deformation. *IEEE Trans. Med. Imaging.* 24: 1334-346.
16. Alberts B., Johnson A., Lewis J., Raff M., Roberts K., Walter P., Molecular Biology of the Cell, Fifth Edition, 2007.
17. http://antoine.frostburg.edu/chem/senese/101/atoms/images/ms3.jpg

18. Seeley E., Caprioli R. (2008). Imaging mass spectrometry: towards clinical diagnostics. *PROTEOMICS - Clinical Applications* 2: 1435-443.
19. Kruse S.A., Rose G.H., Glaser K.J., Manduca A., Felmlee J.P., Clifford R.J.Jr., Ehman R.L.(2008). Magnetic resonance elastography of the brain, *NeuroImage* 39: 231-237.
20. Hirabayashi A., Sakairi M., Koizumi H. (1994). Sonic spray ionization method for atmospheric pressure ionization mass spectroscopy, *Anal.Chem*. 66: 4557-4559.
21. Chen Y.C., Hoger A. (2000). Constitutive functions of elastic materials in finite growth and deformation, *J.Elasticity* 59: 175-193.
22. Kim J. B. (2005). Three-dimensional tissue culture models in cancer biology *J. Biomol. Screening* 15 365–77.
23. Kunz-Schughart L. A., Freyer J. P., Hofstaedter F., Ebner R. (2004). The use of 3-d cultures for high-throughput screening: the multicellular spheroid model *J. Biomol. Screening* 9: 273–285.
24. Mueller-Klieser W. (1987). Multicellular spheroids: a review on cellular aggregates in cancer research *J. Cancer Res. Clin. Oncol.* 113: 101–122.
25. Mueller-Klieser W., Freyer J. P., Sutherland R.M., (1986). Influence of glucose and oxygen supply conditions on the oxygenation of multi-cellular spheroids *Br. J. Cancer* 53: 345–53.
26. Sutherland R.M. (1988). Cell and environment interactions in tumor micro-regions: the multi-cell spheroid model, *Science* 240: 177–184.
27. Sutherland R.M., Carlsson J., Durand R.E., Yuhas J. (1981). Spheroids in cancer research, *Cancer Res.* 41: 2980–2994.
28. Walles T, Weimer M, Linke K, Michaelis J., Mertsching H. (2007). The potential of bioartificial tissues in oncology research and treatment, *Onkologie* 30: 388–394.
29. Lowengrub J.S., Frieboes H.B., Jin F., Chuang Y-L., Li X., Macklin P., Wise S.M., Cristini V. (2010). Nonlinear modeling of cancer: bridging the gap between cells and tumors. *Nonlinearity* 23: 1-91.
30. Greenspan H.P. (1972). Models for the growth of a solid tumor by diffusion *Stud. Appl. Math.* 51: 317–340.
31. Greenspan H.P. (1976). On the growth and stability of cell cultures and solid tumors *J. Theor. Biol.* 56: 229–242.
32. Pham K., Frieboes H.B., Cristini V., Lowengrub J., (2011). Predictions of tumor morphological stability and evaluation against experimental observations, *J. R. Soc. Interface* 54:16-29.
33. Kallel F., Ophir J., Magee K., Krouskop T. (1998). Elastographic imaging of low-contrast elastic modulus distributions in tissue, *Ultrasound Med. Biol.* 24(3): 409-425.
34. Gorenflo R. (1997). Fractional calculus: some numerical methods. *Fractals and Fractional Calculus in Continuum Mechanics CISM Courses and Lectures* 378: 277-290.
35. Adomian, G. (1988). A review of decomposition method in applied mathematics." *Journal of Mathematical Analysis and Applications* 135: 501-544.

36. Drapaca, C.S. Palocaren A.J. (2010). Biomechanical modeling of tumor classification and growtth, *Rev.Roum Sci Techn*.*Mec.Appl*. 55(2): 115-124.
37. Manduca A., Oliphant T.E., Dresner M.A., Mahowald J.L., Kruse S.A., Amromin E., Felmlee J.P., Greenleaf J.F., Ehman R.L. (2001). Magnetic resonance elastography: non-invasive mapping of tissue elasticity, *Med. Imag. Anal*., 5(4): 237-254.
38. Deisboeck, T. S., Zhang, L., Yoon, J., Costa, J. (2009). In silico cancer modeling: is it ready for prime time? *Nature Clin. Practice Oncol*. 6: 34–42.
39. Preziosi, L., Tosin, A. (2009). Multiphase and multiscale trends in cancer modeling. *Math.Mod. Nat. Phenom.* 4: 1–11.
40. Tracqui, P. (2009). Biophysical models of tumor growth. *Rep. Prog. Phys*. 72: 056701.
41. Ventura, A. C., Jackson, T. L., Merajver, S. D. (2009). On the role of cell signaling models in cancer research. *Cancer Res.* 69: 400–402.
42. Swanson, K. R., Bridge, C., Murray, J. D., Alvord, E. C. jr. (2003). Virtual and real brain tumors: using mathematical modeling to quantify glioma growth and invasion. *J. Neuro. Sci.* 216: 1–10.
43. Jbabdi, S., Mandonnet, E., Duffau, H., Capelle, L., Swanson, K. R., Pelegrini-Issac, M.,Guillevin, R., Benali, H. (2005). Simulation of anisotropic growth of low-grade gliomas using diffusion tensor imaging. *Magn. Res. Med.* 54: 616–624.
44. Khain, E., Sander, L. M. (2006). Dynamics and pattern formation in invasive tumor growth. *Phys. Rev. Lett.* 96: 188103.
45. Franks, S. J., Byrne, H. M., King, J. R., Underwood, J. C. E., Lewis, C. E. (2003). Modelling the early growth of ductal carcinoma in situ of the breast. *J. Math. Biol*. 47: 424–452.
46. Franks, S. J., Byrne, H. M., Mudhar, H. S., Underwood,J. C. E., Lewis, C. E. (2003). Mathematical modelling of comedo ductal carcinoma in situ of the breast. *Math. Med. Biol.*20: 277–308.
47. Cristini, V., Lowengrub, J. S., Nie, Q. (2003). Nonlinear simulation of tumor growth. *J. Math.Biol.* 46: 191–224.
48. Cristini, V., Frieboes, H. B., Gatenby, R., Caserta, S., Ferrari, M., Sinek, J. (2005). Morphologic instability and cancer invasion. *Clin. Cancer Res.* 11: 6772–6779.
49. Frieboes, H., Zheng, X., Sun, C., Tromberg, B., Gatenby, R. Cristini, V. (2006). An integrated computational/experimental model of tumor invasion. *Cancer Res*. 66: 1597–1604.
50. Anderson, A. R. A., Quaranta, V. (2008). Integrative mathematical oncology. *Nat. Rev.Cancer* 8: 227–234.
51. Byrne, H. M., Chaplain, M. A. J. (1995). Growth of nonnecrotic tumors in the presence and absence of inhibitors. *Math. Biosciences* 130: 151–181.

52. Byrne, H. M., Chaplain, M. A. J. (1996). Modelling the role of cell–cell-adhesion in the growth and development of carcinomas. *Math.Comput.Modelling* 24: 1–17.
53. Byrne, H. M., Chaplain, M. A. J. (1997). Free boundary value problems associated with the growth and development of multi-cellular spheroids. *Eur. J. Appl. Math*. 8: 639–658.
54. Friedman, A., Reitich, F. (1999). Analysis of a mathematical model for the growth of tumors. *J. Math. Biol.* 38: 262–284.
55. Friedman, A., Bellomo, N., Maini, P. K. (2007). Mathematical analysis and challenges arising from models of tumor growth. *Math. Models Meth. Appl. Sci*. 17: 1751–1772.
56. King, J. R., Franks, S. J. (2004). Mathematical analysis of some multi-dimensional tissue growth models. *Euro.J. Appl. Math.* 15: 273–295.
57. King, J. R., Franks, S. J. (2007). Mathematical modelling of nutrient-limited tissue growth. *Int. Numer. Math.* 154: 273–282.
58. Franks, S. J., King, J. R. (2003). Interactions between a uniformly proliferating tumor and its surrounding: uniform material properties. *Math. Med. Biol*. 20: 47–89.
59. Jumarie G. (2006). New stochastic fractional models for Malthusian growth, the Poissonian birth process and optimal management of populations, *Mathematical and Computer Modelling*, 44 (3-4): 213-254.
60. Geyikli T., Kaya D. (2005). Comparison of the solutions obtained by B-spline FEM and ADM of KdV equation, *Appl.Math.Comp.* 169(1): 146-156.
61. El-Wakil S.A., Elhanbaly A., Abdou M.A. (2006). Adomian decomposition method for solving fractional nonlinear differential equations, *Appl.Math.Comp.* 182:313-324.

Appendix – Computational Codes

MATLAB Codes

```
%%%%%%%%%%%%%%%%%%%%%%%%%%%%%
% This program builds elastograms (images of the Young modulus) at a certain mass-
%per-charge (m/z) ratio using images of mass spectroscopy.
%%%%%%%%%%%%%%%%%%%%%%%%%%%%%
m=imread('5826.jpg');
n=imread('7380.jpg');
o=imread('10625.jpg');
p=imread('10092.jpg');
q=imread('11068.jpg');
b=rgb2gray(m);
c=rgb2gray(n);
d=rgb2gray(o);
e=rgb2gray(p);
f=rgb2gray(q);
newb=double(b);
newc=double(c);
newd=double(d);
newe=double(e);
newf=double(f);
figure, imagesc(newb);
impixelinfo;
alpha_b=0.6+log(1/5826);
alpha_c=0.6+log(1/7380);
alpha_d=0.6+log(1/10625);
alpha_e=0.6+log(1/10092);
alpha_f=0.6+log(1/11068);
Young_Modulus=newb.^alpha_b+newc.^alpha_c+newd.^alpha_d+newe.^alpha_e+newf.
^alpha_f;
figure, imagesc(Young_Modulus); %elastogram
22
%%%%%%%%%%%%%%%%%%%%%%%%%%%%%
%This program builds elastograms (images of the Young modulus) at
%a certain mass-per-charge (m/z) ratio using images of mass spectroscopy.
%%%%%%%%%%%%%%%%%%%%%%%%%%%%%
m=imread('5826.jpg');
n=imread('7380.jpg');
o=imread('10625.jpg');
p=imread('10092.jpg');
q=imread('11068.jpg');
b=rgb2gray(m);
c=rgb2gray(n);
d=rgb2gray(o);
e=rgb2gray(p);
f=rgb2gray(q);
newb=double(b);
newc=double(c);
```

```
newd=double(d);
newe=double(e);
newf=double(f);
figure, imagesc(newb);
impixelinfo;
alpha=0.6;
Young_Modulus=newb.^alpha+newc.^alpha+newd.^alpha+newe.^alpha+newf.^alpha;
figure, imagesc(Young_Modulus); %elastogram
23
%%%%%%%%%%%%%%%%%%%%%
% This code is for the mechano-growth model.
%%%%%%%%%%%%%%%%%%%%%
clear all
clc
K0=1;
gamma=1.3*10^(-26); %m^3
kB=1.3*10^(-23); %m^2*Kg/(s^2*K)
T=298; %K
alpha=gamma/(kB*T);
E_lg=30*10^(3); %Pa=Kg/(s^2*m); low grade
E_hg=40*10^3; %high grade
K_lg=K0*exp(-alpha*E_lg);
K_hg=K0*exp(-alpha*E_hg);
lambda=1;
beta_lg=K_lg*exp(alpha*E_lg*lambda);
beta_hg=K_hg*exp(alpha*E_hg*lambda);
t=0:0.001:1; %normalized time scale
%the growth functions are dimensionless
g_lg=exp(beta_lg/(alpha*E_lg*lambda).*(1-exp( beta_lg*alpha*E_lg*lambda.*t)));
g_hg=exp(beta_hg/(alpha*E_hg*lambda).*(1-exp(-beta_hg*alpha*E_hg*lambda.*t)));
plot(t, g_lg, 'b', t, g_hg, 'r', 'LineWidth', 2)
```

Mechano Growth Modelling Using Adomian Polynomials

Lambda at various values for high grade and low grade tumors:

- **Explanation of the constants used in the model:**

  Gamma = 1.3*10^(-26) [Constant that depends on the bio-chemical reactions involved in growth process]

  k = 1.3*10^(-23) [Boltzman constant]

  T = 298 K [Absolute temprature]

  Yong_lg = 30*10^3 Pa [Youngs modulus of a low-grade tumor tissue]

  Young_hg = 40*10^3 Pa [Youngs modulus of a high-grade tumor tissue]

```
Gam = 1.3 * 10^(-26)
```

1.3×10^{-26}

```
k = 1.3 * 10^(-23)
```

1.3×10^{-23}

```
T = 298
```

298

```
Younglg = 30 * 10^3
```

30 000

```
Younghg = 40 * 10^3
```

40 000

```
Lamb = 4
```

4

```
Clear[Azero, Aone, Atwo, Athree, Rzero, Rone, Rtwo]
```

```
Rzero = 1 (*This is the initial condition*)
```

1

```
Azerolg = Exp[Gam * Younglg * ((Lamb / Rzero) - 1) / (k * T)] * Rzero
```

1.35258

```
Azerohg = Exp[Gam * Younghg * ((Lamb / Rzero) - 1) / (k * T)] * Rzero
```

1.49583

$$\text{Ronelg} = \left(\int \text{Azerolg}\, dt\right)$$

1.35258 t

$$\text{Ronehg} = \left(\int \text{Azerohg}\, dt\right)$$

1.49583 t

$$\text{Aonelg} = \text{Ronelg}\left(e^{\frac{\text{Gam}\left(-1+\frac{\text{Lamb}}{\text{Rzero}}\right)\text{Younglg}}{k\,T}} - \frac{e^{\frac{\text{Gam}\left(-1+\frac{\text{Lamb}}{\text{Rzero}}\right)\text{Younglg}}{k\,T}}\,\text{Gam Lamb Younglg}}{k\,\text{Rzero}\,T}\right)$$

1.09277 t

$$\text{Aonehg} = \text{Ronehg}\left(e^{\frac{\text{Gam}\left(-1+\frac{\text{Lamb}}{\text{Rzero}}\right)\text{Younghg}}{k\,T}} - \frac{e^{\frac{\text{Gam}\left(-1+\frac{\text{Lamb}}{\text{Rzero}}\right)\text{Younghg}}{k\,T}}\,\text{Gam Lamb Younghg}}{k\,\text{Rzero}\,T}\right)$$

1.03617 t

$$\text{Rtwolg} = \int \text{Aonelg}\, dt$$

0.546386 t^2

$$\text{Rtwohg} = \int \text{Aonehg}\, dt$$

0.518084 t^2

$$\text{Atwolg} = \text{Rtwolg}\left(e^{\frac{\text{Gam}\left(-1+\frac{\text{Lamb}}{\text{Rzero}}\right)\text{Younglg}}{k\,T}} - \frac{e^{\frac{\text{Gam}\left(-1+\frac{\text{Lamb}}{\text{Rzero}}\right)\text{Younglg}}{k\,T}}\,\text{Gam Lamb Younglg}}{k\,\text{Rzero}\,T}\right) +$$
$$\frac{1}{2}\,\text{Ronelg}^2\left(-\frac{2\,e^{\frac{\text{Gam}\left(-1+\frac{\text{Lamb}}{\text{Rzero}}\right)\text{Younglg}}{k\,T}}\,\text{Gam Lamb Younglg}}{k\,\text{Rzero}^2\,T} +$$
$$\text{Rzero}\left(\frac{2\,e^{\frac{\text{Gam}\left(-1+\frac{\text{Lamb}}{\text{Rzero}}\right)\text{Younglg}}{k\,T}}\,\text{Gam Lamb Younglg}}{k\,\text{Rzero}^3\,T} + \frac{e^{\frac{\text{Gam}\left(-1+\frac{\text{Lamb}}{\text{Rzero}}\right)\text{Younglg}}{k\,T}}\,\text{Gam}^2\,\text{Lamb}^2\,\text{Younglg}^2}{k^2\,\text{Rzero}^4\,T^2}\right)\right)$$

0.64206 t^2

$$\text{Atwohg} = \text{Rtwohg}\left(e^{\frac{\text{Gam}\left(-1+\frac{\text{Lamb}}{\text{Rzero}}\right)\text{Younghg}}{\text{k T}}} - \frac{e^{\frac{\text{Gam}\left(-1+\frac{\text{Lamb}}{\text{Rzero}}\right)\text{Younghg}}{\text{k T}}}\text{Gam Lamb Younghg}}{\text{k Rzero T}}\right) +$$

$$\frac{1}{2}\text{Ronehg}^2\left(-\frac{2\,e^{\frac{\text{Gam}\left(-1+\frac{\text{Lamb}}{\text{Rzero}}\right)\text{Younghg}}{\text{k T}}}\text{Gam Lamb Younghg}}{\text{k Rzero}^2\text{ T}} +\right.$$

$$\left.\text{Rzero}\left(\frac{2\,e^{\frac{\text{Gam}\left(-1+\frac{\text{Lamb}}{\text{Rzero}}\right)\text{Younghg}}{\text{k T}}}\text{Gam Lamb Younghg}}{\text{k Rzero}^3\text{ T}} + \frac{e^{\frac{\text{Gam}\left(-1+\frac{\text{Lamb}}{\text{Rzero}}\right)\text{Younghg}}{\text{k T}}}\text{Gam}^2\text{ Lamb}^2\text{ Younghg}^2}{\text{k}^2\text{ Rzero}^4\text{ T}^2}\right)\right)$$

$0.841301\,t^2$

$$\text{Rthreelg} = \left(\int \text{Atwolg}\,dt\right)$$

$0.21402\,t^3$

$$\text{Rthreehg} = \left(\int \text{Atwohg}\,dt\right)$$

$0.280434\,t^3$

$$\text{Athreelg} = \text{Rthreelg}\left(e^{\frac{\text{Gam}\left(-1+\frac{\text{Lamb}}{\text{Rzero}}\right)\text{Younglg}}{k\,T}} - \frac{e^{\frac{\text{Gam}\left(-1+\frac{\text{Lamb}}{\text{Rzero}}\right)\text{Younglg}}{k\,T}}\,\text{Gam Lamb Younglg}}{k\,\text{Rzero}\,T}\right) +$$

$$\text{Ronelg Rtwolg}\left(-\frac{2\,e^{\frac{\text{Gam}\left(-1+\frac{\text{Lamb}}{\text{Rzero}}\right)\text{Younglg}}{k\,T}}\,\text{Gam Lamb Younglg}}{k\,\text{Rzero}^2\,T} +\right.$$

$$\text{Rzero}\left(\frac{2\,e^{\frac{\text{Gam}\left(-1+\frac{\text{Lamb}}{\text{Rzero}}\right)\text{Younglg}}{k\,T}}\,\text{Gam Lamb Younglg}}{k\,\text{Rzero}^3\,T} + \frac{e^{\frac{\text{Gam}\left(-1+\frac{\text{Lamb}}{\text{Rzero}}\right)\text{Younglg}}{k\,T}}\,\text{Gam}^2\,\text{Lamb}^2\,\text{Younglg}^2}{k^2\,\text{Rzero}^4\,T^2}\right)\right) +$$

$$\frac{1}{6}\,\text{Ronelg}^3\left(3\left(\frac{2\,e^{\frac{\text{Gam}\left(-1+\frac{\text{Lamb}}{\text{Rzero}}\right)\text{Younglg}}{k\,T}}\,\text{Gam Lamb Younglg}}{k\,\text{Rzero}^3\,T} + \frac{e^{\frac{\text{Gam}\left(-1+\frac{\text{Lamb}}{\text{Rzero}}\right)\text{Younglg}}{k\,T}}\,\text{Gam}^2\,\text{Lamb}^2\,\text{Younglg}^2}{k^2\,\text{Rzero}^4\,T^2}\right) +\right.$$

$$\text{Rzero}\left(-\frac{6\,e^{\frac{\text{Gam}\left(-1+\frac{\text{Lamb}}{\text{Rzero}}\right)\text{Younglg}}{k\,T}}\,\text{Gam Lamb Younglg}}{k\,\text{Rzero}^4\,T} -\right.$$

$$\left.\left.\left.\frac{6\,e^{\frac{\text{Gam}\left(-1+\frac{\text{Lamb}}{\text{Rzero}}\right)\text{Younglg}}{k\,T}}\,\text{Gam}^2\,\text{Lamb}^2\,\text{Younglg}^2}{k^2\,\text{Rzero}^5\,T^2} - \frac{e^{\frac{\text{Gam}\left(-1+\frac{\text{Lamb}}{\text{Rzero}}\right)\text{Younglg}}{k\,T}}\,\text{Gam}^3\,\text{Lamb}^3\,\text{Younglg}^3}{k^3\,\text{Rzero}^6\,T^3}\right)\right)\right)$$

$$0.027212\,t^3$$

$$\text{Athreehg} = \text{Rthreehg}\left(e^{\frac{\text{Gam}\left(-1+\frac{\text{Lamb}}{\text{Rzero}}\right)\text{Younghg}}{\text{k T}}} - \frac{e^{\frac{\text{Gam}\left(-1+\frac{\text{Lamb}}{\text{Rzero}}\right)\text{Younghg}}{\text{k T}}}\text{Gam Lamb Younghg}}{\text{k Rzero T}}\right) +$$

$$\text{Ronehg Rtwohg}\left(-\frac{2\,e^{\frac{\text{Gam}\left(-1+\frac{\text{Lamb}}{\text{Rzero}}\right)\text{Younghg}}{\text{k T}}}\text{Gam Lamb Younghg}}{\text{k Rzero}^2\,\text{T}} +\right.$$

$$\left.\text{Rzero}\left(\frac{2\,e^{\frac{\text{Gam}\left(-1+\frac{\text{Lamb}}{\text{Rzero}}\right)\text{Younghg}}{\text{k T}}}\text{Gam Lamb Younghg}}{\text{k Rzero}^3\,\text{T}} + \frac{e^{\frac{\text{Gam}\left(-1+\frac{\text{Lamb}}{\text{Rzero}}\right)\text{Younghg}}{\text{k T}}}\text{Gam}^2\,\text{Lamb}^2\,\text{Younghg}^2}{\text{k}^2\,\text{Rzero}^4\,\text{T}^2}\right)\right) +$$

$$\frac{1}{6}\text{Ronehg}^3\left(3\left(\frac{2\,e^{\frac{\text{Gam}\left(-1+\frac{\text{Lamb}}{\text{Rzero}}\right)\text{Younghg}}{\text{k T}}}\text{Gam Lamb Younghg}}{\text{k Rzero}^3\,\text{T}} + \frac{e^{\frac{\text{Gam}\left(-1+\frac{\text{Lamb}}{\text{Rzero}}\right)\text{Younghg}}{\text{k T}}}\text{Gam}^2\,\text{Lamb}^2\,\text{Younghg}^2}{\text{k}^2\,\text{Rzero}^4\,\text{T}^2}\right) +\right.$$

$$\left.\text{Rzero}\left(-\frac{6\,e^{\frac{\text{Gam}\left(-1+\frac{\text{Lamb}}{\text{Rzero}}\right)\text{Younghg}}{\text{k T}}}\text{Gam Lamb Younghg}}{\text{k Rzero}^4\,\text{T}} -\right.\right.$$

$$\left.\left.\frac{6\,e^{\frac{\text{Gam}\left(-1+\frac{\text{Lamb}}{\text{Rzero}}\right)\text{Younghg}}{\text{k T}}}\text{Gam}^2\,\text{Lamb}^2\,\text{Younghg}^2}{\text{k}^2\,\text{Rzero}^5\,\text{T}^2} - \frac{e^{\frac{\text{Gam}\left(-1+\frac{\text{Lamb}}{\text{Rzero}}\right)\text{Younghg}}{\text{k T}}}\text{Gam}^3\,\text{Lamb}^3\,\text{Younghg}^3}{\text{k}^3\,\text{Rzero}^6\,\text{T}^3}\right)\right)$$

$$-0.322343\,t^3$$

$$\text{Rfourlg} = \left(\int \text{Athreelg}\,dt\right)$$

$$0.00680301\,t^4$$

$$\text{Rfourhg} = \left(\int \text{Athreehg}\,dt\right)$$

$$-0.0805858\,t^4$$

$$\text{Rhg} = \text{Rzero} + \text{Ronehg} + \text{Rtwohg} + \text{Rthreehg} + \text{Rfourhg}$$

$$1 + 1.49583\,t + 0.518084\,t^2 + 0.280434\,t^3 - 0.0805858\,t^4$$

$$\text{Rlg} = \text{Rzero} + \text{Ronelg} + \text{Rtwolg} + \text{Rthreelg} + \text{Rfourlg}$$

$$1 + 1.35258\,t + 0.546386\,t^2 + 0.21402\,t^3 + 0.00680301\,t^4$$

```
Plot[{Rhg, Rlg}, {t, 0, 1}, PlotStyle → {Thickness[0.008], {Red}, {RGBColor[0.3, 0, 0.7]}},
 AxesLabel → {Time , Growth}, LabelStyle → Directive[Blue, Bold]]
```

Mechano Growth Modelling Using Adomian Polynomials

Lambda at various values for high grade and low grade tumors:

- **Explanation of the constants used in the model:**

  Gamma = 1.3*10^(-26) [Constant that depends on the bio-chemical reactions involved in growth process]

  k = 1.3*10^(-23) [Boltzman constant]

  T = 298 K [Absolute temprature]

  Yong_lg = 30*10^3 Pa [Youngs modulus of a low-grade tumor tissue]

  Young_hg = 40*10^3 Pa [Youngs modulus of a high-grade tumor tissue]

```
alpha = 0.9
```

0.9

```
Gam = 1.3 * 10^(-26)
```

1.3×10^{-26}

```
k = 1.3 * 10^(-23)
```

1.3×10^{-23}

```
T = 298
```

298

```
Younglg = 30 * 10^3
```

30 000

```
Younghg = 40 * 10^3
```

40 000

```
Lamb = 5
```

5

```
Clear[Azero, Aone, Atwo, Athree, Rzero, Rone, Rtwo]
```

```
Rzero = 1 (*This is the initial condition*)
```

1

```
Azerolg = Exp[Gam * Younglg * ((Lamb / Rzero) - 1) / (k * T)] * Rzero
```

1.49583

```
Azerohg = Exp[Gam * Younghg * ((Lamb / Rzero) - 1) / (k * T)] * Rzero
```

1.71072

$$\text{Ronelg} = (1 / \Gamma[\text{alpha}]) \int_0^t \text{Azerolg} / ((t - s)^{(1 - \text{alpha})})\, ds$$

$$1.39977\ \text{If}\left[t > 0,\ 1.11111\ t^{0.9},\ \text{Integrate}\left[\frac{1}{(-s+t)^{0.1}},\ \{s, 0, t\},\ \text{Assumptions} \to t \le 0\right]\right]$$

$$\text{Ronehg} = (1 / \Gamma[\text{alpha}]) \int_0^t \text{Azerohg} / ((t - s)^{(1 - \text{alpha})})\, ds$$

$$1.60085\ \text{If}\left[t > 0,\ 1.11111\ t^{0.9},\ \text{Integrate}\left[\frac{1}{(-s+t)^{0.1}},\ \{s, 0, t\},\ \text{Assumptions} \to t \le 0\right]\right]$$

$$\text{Aonelg} = \text{Ronelg}\left(e^{\frac{\text{Gam}\left(-1+\frac{\text{Lamb}}{\text{Rzero}}\right)\text{Younglg}}{k\,T}} - \frac{e^{\frac{\text{Gam}\left(-1+\frac{\text{Lamb}}{\text{Rzero}}\right)\text{Younglg}}{k\,T}}\,\text{Gam Lamb Younglg}}{k\,\text{Rzero}\,T}\right)$$

$$1.03989\ \text{If}\left[t > 0,\ 1.11111\ t^{0.9},\ \text{Integrate}\left[\frac{1}{(-s+t)^{0.1}},\ \{s, 0, t\},\ \text{Assumptions} \to t \le 0\right]\right]$$

$$\text{Aonehg} = \text{Ronehg}\left(e^{\frac{\text{Gam}\left(-1+\frac{\text{Lamb}}{\text{Rzero}}\right)\text{Younghg}}{k\,T}} - \frac{e^{\frac{\text{Gam}\left(-1+\frac{\text{Lamb}}{\text{Rzero}}\right)\text{Younghg}}{k\,T}}\,\text{Gam Lamb Younghg}}{k\,\text{Rzero}\,T}\right)$$

$$0.900616\ \text{If}\left[t > 0,\ 1.11111\ t^{0.9},\ \text{Integrate}\left[\frac{1}{(-s+t)^{0.1}},\ \{s, 0, t\},\ \text{Assumptions} \to t \le 0\right]\right]$$

$$\text{Rtwolg} = (1 / \Gamma[\text{alpha}]) \int_0^t \text{Aonelg} / ((t - s)^{(1 - \text{alpha})})\, ds$$

$$0.973104\ \text{If}\left[t > 0,\ 1.11111\ t^{0.9},\ \text{Integrate}\left[\frac{1}{(-s+t)^{0.1}},\ \{s, 0, t\},\ \text{Assumptions} \to t \le 0\right]\right]^2$$

$$\text{Rtwohg} = (1 / \text{Gamma}[\text{alpha}]) \int_0^t \text{Aonehg} / ((t - s)^{\wedge}(1 - \text{alpha}))\, ds$$

$$0.842777\ \text{If}\left[t > 0,\ 1.11111\ t^{0.9},\ \text{Integrate}\left[\frac{1}{(-s+t)^{0.1}},\ \{s,\ 0,\ t\},\ \text{Assumptions} \to t \le 0\right]\right]^2$$

$$\text{Atwolg} = \text{Rtwolg}\left(e^{\frac{\text{Gam}\left(-1+\frac{\text{Lamb}}{\text{Rzero}}\right)\text{Younglg}}{k\,T}} - \frac{e^{\frac{\text{Gam}\left(-1+\frac{\text{Lamb}}{\text{Rzero}}\right)\text{Younglg}}{k\,T}}\,\text{Gam Lamb Younglg}}{k\,\text{Rzero}\,T}\right) +$$

$$\frac{1}{2}\,\text{Ronelg}^2\left(-\frac{2\,e^{\frac{\text{Gam}\left(-1+\frac{\text{Lamb}}{\text{Rzero}}\right)\text{Younglg}}{k\,T}}\,\text{Gam Lamb Younglg}}{k\,\text{Rzero}^2\,T} + \text{Rzero}\left(\frac{2\,e^{\frac{\text{Gam}\left(-1+\frac{\text{Lamb}}{\text{Rzero}}\right)\text{Younglg}}{k\,T}}\,\text{Gam Lamb Younglg}}{k\,\text{Rzero}^3\,T} + \frac{e^{\frac{\text{Gam}\left(-1+\frac{\text{Lamb}}{\text{Rzero}}\right)\text{Younglg}}{k\,T}}\,\text{Gam}^2\,\text{Lamb}^2\,\text{Younglg}^2}{k^2\,\text{Rzero}^4\,T^2}\right)\right)$$

$$1.09421\ \text{If}\left[t > 0,\ 1.11111\ t^{0.9},\ \text{Integrate}\left[\frac{1}{(-s+t)^{0.1}},\ \{s,\ 0,\ t\},\ \text{Assumptions} \to t \le 0\right]\right]^2$$

$$\text{Atwohg} = \text{Rtwohg}\left(e^{\frac{\text{Gam}\left(-1+\frac{\text{Lamb}}{\text{Rzero}}\right)\text{Younghg}}{k\,T}} - \frac{e^{\frac{\text{Gam}\left(-1+\frac{\text{Lamb}}{\text{Rzero}}\right)\text{Younghg}}{k\,T}}\,\text{Gam Lamb Younghg}}{k\,\text{Rzero}\,T}\right) +$$

$$\frac{1}{2}\,\text{Ronehg}^2\left(-\frac{2\,e^{\frac{\text{Gam}\left(-1+\frac{\text{Lamb}}{\text{Rzero}}\right)\text{Younghg}}{k\,T}}\,\text{Gam Lamb Younghg}}{k\,\text{Rzero}^2\,T} + \text{Rzero}\left(\frac{2\,e^{\frac{\text{Gam}\left(-1+\frac{\text{Lamb}}{\text{Rzero}}\right)\text{Younghg}}{k\,T}}\,\text{Gam Lamb Younghg}}{k\,\text{Rzero}^3\,T} + \frac{e^{\frac{\text{Gam}\left(-1+\frac{\text{Lamb}}{\text{Rzero}}\right)\text{Younghg}}{k\,T}}\,\text{Gam}^2\,\text{Lamb}^2\,\text{Younghg}^2}{k^2\,\text{Rzero}^4\,T^2}\right)\right)$$

$$1.4615\ \text{If}\left[t > 0,\ 1.11111\ t^{0.9},\ \text{Integrate}\left[\frac{1}{(-s+t)^{0.1}},\ \{s,\ 0,\ t\},\ \text{Assumptions} \to t \le 0\right]\right]^2$$

$$\text{Rthreelg} = (1 / \text{Gamma}[\text{alpha}]) \int_0^t \text{Atwolg} / ((t - s)^{\wedge}(1 - \text{alpha}))\, ds$$

$$1.02394\ \text{If}\left[t > 0,\ 1.11111\ t^{0.9},\ \text{Integrate}\left[\frac{1}{(-s+t)^{0.1}},\ \{s,\ 0,\ t\},\ \text{Assumptions} \to t \le 0\right]\right]^3$$

$$\text{Rthreehg} = (1 / \text{Gamma}[\text{alpha}]) \int_0^t \text{Atwohg} / ((t - s)^{\wedge}(1 - \text{alpha}))\, ds$$

$$1.36764\ \text{If}\left[t > 0,\ 1.11111\ t^{0.9},\ \text{Integrate}\left[\frac{1}{(-s+t)^{0.1}},\ \{s,\ 0,\ t\},\ \text{Assumptions} \to t \le 0\right]\right]^3$$

$$\text{Athreelg} = \text{Rthreelg}\left(e^{\frac{\text{Gam}\left(-1+\frac{\text{Lamb}}{\text{Rzero}}\right)\text{Younglg}}{k\,T}} - \frac{e^{\frac{\text{Gam}\left(-1+\frac{\text{Lamb}}{\text{Rzero}}\right)\text{Younglg}}{k\,T}}\,\text{Gam Lamb Younglg}}{k\,\text{Rzero}\,T}\right) +$$

$$\text{Ronelg Rtwolg}\left(-\frac{2\,e^{\frac{\text{Gam}\left(-1+\frac{\text{Lamb}}{\text{Rzero}}\right)\text{Younglg}}{k\,T}}\,\text{Gam Lamb Younglg}}{k\,\text{Rzero}^2\,T} +\right.$$

$$\left.\text{Rzero}\left(\frac{2\,e^{\frac{\text{Gam}\left(-1+\frac{\text{Lamb}}{\text{Rzero}}\right)\text{Younglg}}{k\,T}}\,\text{Gam Lamb Younglg}}{k\,\text{Rzero}^3\,T} + \frac{e^{\frac{\text{Gam}\left(-1+\frac{\text{Lamb}}{\text{Rzero}}\right)\text{Younglg}}{k\,T}}\,\text{Gam}^2\,\text{Lamb}^2\,\text{Younglg}^2}{k^2\,\text{Rzero}^4\,T^2}\right)\right) +$$

$$\frac{1}{6}\,\text{Ronelg}^3\left(3\left(\frac{2\,e^{\frac{\text{Gam}\left(-1+\frac{\text{Lamb}}{\text{Rzero}}\right)\text{Younglg}}{k\,T}}\,\text{Gam Lamb Younglg}}{k\,\text{Rzero}^3\,T} + \frac{e^{\frac{\text{Gam}\left(-1+\frac{\text{Lamb}}{\text{Rzero}}\right)\text{Younglg}}{k\,T}}\,\text{Gam}^2\,\text{Lamb}^2\,\text{Younglg}^2}{k^2\,\text{Rzero}^4\,T^2}\right) +\right.$$

$$\left.\text{Rzero}\left(-\frac{6\,e^{\frac{\text{Gam}\left(-1+\frac{\text{Lamb}}{\text{Rzero}}\right)\text{Younglg}}{k\,T}}\,\text{Gam Lamb Younglg}}{k\,\text{Rzero}^4\,T} -\right.\right.$$

$$\left.\left.\frac{6\,e^{\frac{\text{Gam}\left(-1+\frac{\text{Lamb}}{\text{Rzero}}\right)\text{Younglg}}{k\,T}}\,\text{Gam}^2\,\text{Lamb}^2\,\text{Younglg}^2}{k^2\,\text{Rzero}^5\,T^2} - \frac{e^{\frac{\text{Gam}\left(-1+\frac{\text{Lamb}}{\text{Rzero}}\right)\text{Younglg}}{k\,T}}\,\text{Gam}^3\,\text{Lamb}^3\,\text{Younglg}^3}{k^3\,\text{Rzero}^6\,T^3}\right)\right)$$

$$0.669992\,\text{If}\left[t > 0,\ 1.11111\,t^{0.9},\ \text{Integrate}\left[\frac{1}{(-s+t)^{0.1}},\ \{s,\ 0,\ t\},\ \text{Assumptions} \to t \le 0\right]\right]^3$$

$$\text{Athreehg} = \text{Rthreehg}\left(e^{\frac{\text{Gam}\left(-1+\frac{\text{Lamb}}{\text{Rzero}}\right)\text{Younghg}}{k\,T}} - \frac{e^{\frac{\text{Gam}\left(-1+\frac{\text{Lamb}}{\text{Rzero}}\right)\text{Younghg}}{k\,T}}\,\text{Gam Lamb Younghg}}{k\,\text{Rzero}\,T}\right) +$$

$$\text{Ronehg Rtwohg}\left(-\frac{2\,e^{\frac{\text{Gam}\left(-1+\frac{\text{Lamb}}{\text{Rzero}}\right)\text{Younghg}}{k\,T}}\,\text{Gam Lamb Younghg}}{k\,\text{Rzero}^2\,T} +\right.$$

$$\left.\text{Rzero}\left(\frac{2\,e^{\frac{\text{Gam}\left(-1+\frac{\text{Lamb}}{\text{Rzero}}\right)\text{Younghg}}{k\,T}}\,\text{Gam Lamb Younghg}}{k\,\text{Rzero}^3\,T} + \frac{e^{\frac{\text{Gam}\left(-1+\frac{\text{Lamb}}{\text{Rzero}}\right)\text{Younghg}}{k\,T}}\,\text{Gam}^2\,\text{Lamb}^2\,\text{Younghg}^2}{k^2\,\text{Rzero}^4\,T^2}\right)\right) +$$

$$\frac{1}{6}\,\text{Ronehg}^3\left(3\left(\frac{2\,e^{\frac{\text{Gam}\left(-1+\frac{\text{Lamb}}{\text{Rzero}}\right)\text{Younghg}}{k\,T}}\,\text{Gam Lamb Younghg}}{k\,\text{Rzero}^3\,T} + \frac{e^{\frac{\text{Gam}\left(-1+\frac{\text{Lamb}}{\text{Rzero}}\right)\text{Younghg}}{k\,T}}\,\text{Gam}^2\,\text{Lamb}^2\,\text{Younghg}^2}{k^2\,\text{Rzero}^4\,T^2}\right) +\right.$$

$$\left.\text{Rzero}\left(-\frac{6\,e^{\frac{\text{Gam}\left(-1+\frac{\text{Lamb}}{\text{Rzero}}\right)\text{Younghg}}{k\,T}}\,\text{Gam Lamb Younghg}}{k\,\text{Rzero}^4\,T} -\right.\right.$$

$$\left.\left.\frac{6\,e^{\frac{\text{Gam}\left(-1+\frac{\text{Lamb}}{\text{Rzero}}\right)\text{Younghg}}{k\,T}}\,\text{Gam}^2\,\text{Lamb}^2\,\text{Younghg}^2}{k^2\,\text{Rzero}^5\,T^2} - \frac{e^{\frac{\text{Gam}\left(-1+\frac{\text{Lamb}}{\text{Rzero}}\right)\text{Younghg}}{k\,T}}\,\text{Gam}^3\,\text{Lamb}^3\,\text{Younghg}^3}{k^3\,\text{Rzero}^6\,T^3}\right)\right)$$

$$-0.125215\,\text{If}\left[t > 0,\ 1.11111\,t^{0.9},\ \text{Integrate}\left[\frac{1}{(-s+t)^{0.1}},\ \{s,\ 0,\ t\},\ \text{Assumptions} \to t \le 0\right]\right]^3$$

$$\text{Rfourlg} = (1 / \text{Gamma}[\text{alpha}])\int_0^t \text{Athreelg} / ((t-s)\,\text{^}\,(1-\text{alpha}))\,ds$$

$$0.626964\,\text{If}\left[t > 0,\ 1.11111\,t^{0.9},\ \text{Integrate}\left[\frac{1}{(-s+t)^{0.1}},\ \{s,\ 0,\ t\},\ \text{Assumptions} \to t \le 0\right]\right]^4$$

$$\text{Rfourhg} = (1 / \text{Gamma}[\text{alpha}])\int_0^t \text{Athreehg} / ((t-s)\,\text{^}\,(1-\text{alpha}))\,ds$$

$$-0.117173\,\text{If}\left[t > 0,\ 1.11111\,t^{0.9},\ \text{Integrate}\left[\frac{1}{(-s+t)^{0.1}},\ \{s,\ 0,\ t\},\ \text{Assumptions} \to t \le 0\right]\right]^4$$

Rhg = Rzero + Ronehg + Rtwohg + Rthreehg + Rfourhg

$$1 + 1.60085\ \text{If}\left[t > 0,\ 1.11111\ t^{0.9},\ \text{Integrate}\left[\frac{1}{(-s+t)^{0.1}},\ \{s, 0, t\},\ \text{Assumptions} \to t \le 0\right]\right] +$$
$$0.842777\ \text{If}\left[t > 0,\ 1.11111\ t^{0.9},\ \text{Integrate}\left[\frac{1}{(-s+t)^{0.1}},\ \{s, 0, t\},\ \text{Assumptions} \to t \le 0\right]\right]^2 +$$
$$1.36764\ \text{If}\left[t > 0,\ 1.11111\ t^{0.9},\ \text{Integrate}\left[\frac{1}{(-s+t)^{0.1}},\ \{s, 0, t\},\ \text{Assumptions} \to t \le 0\right]\right]^3 -$$
$$0.117173\ \text{If}\left[t > 0,\ 1.11111\ t^{0.9},\ \text{Integrate}\left[\frac{1}{(-s+t)^{0.1}},\ \{s, 0, t\},\ \text{Assumptions} \to t \le 0\right]\right]^4$$

Rlg = Rzero + Ronelg + Rtwolg + Rthreelg + Rfourlg

$$1 + 1.39977\ \text{If}\left[t > 0,\ 1.11111\ t^{0.9},\ \text{Integrate}\left[\frac{1}{(-s+t)^{0.1}},\ \{s, 0, t\},\ \text{Assumptions} \to t \le 0\right]\right] +$$
$$0.973104\ \text{If}\left[t > 0,\ 1.11111\ t^{0.9},\ \text{Integrate}\left[\frac{1}{(-s+t)^{0.1}},\ \{s, 0, t\},\ \text{Assumptions} \to t \le 0\right]\right]^2 +$$
$$1.02394\ \text{If}\left[t > 0,\ 1.11111\ t^{0.9},\ \text{Integrate}\left[\frac{1}{(-s+t)^{0.1}},\ \{s, 0, t\},\ \text{Assumptions} \to t \le 0\right]\right]^3 +$$
$$0.626964\ \text{If}\left[t > 0,\ 1.11111\ t^{0.9},\ \text{Integrate}\left[\frac{1}{(-s+t)^{0.1}},\ \{s, 0, t\},\ \text{Assumptions} \to t \le 0\right]\right]^4$$

```
Plot[{Rhg, Rlg}, {t, 0, 1},
 PlotStyle → { Thickness[0.008], {Red}, {RGBColor[0.3, 0, 0.7], Thick}},
 AxesLabel → {Time , Growth}, LabelStyle → Directive[Blue, Bold]]
```

Academic Vita

Antony J. Palocaren

1505 Anna Avenue
West Mifflin, PA 15122

(412)-596-2224
ajp5099@psu.edu

Education:

The Pennsylvania State University
Master of Science, expected May 2011
Major: Engineering Mechanics

Publications:

- **A novel mechanical model for tumor classification,**
  Proceedings of SISOM 2010 and session of the commission of acoustics, Pg:15-18

- **Biomechanical modeling of tumor classification and growth**
  Rev. Roum Sci Techn – Mec Appl Tome 55(12), Pg: 115-124, 2010

Presentations:

- **Workshop on mathematical oncology III, 2010**
  Centre for the mathematical medicine and fields institute

- **SIAM conference on mathematical aspects of material sciences, 2010**

- **ESM Today, 2011**
  Department of Engineering Science & Mechanics, The Pennsylvania State University

- **CERS 2011**
  College of Engineering Research Symposium, The Pennsylvania State University

Academic Awards & Accomplishments:

Military Officers Association of America Medal of Honor
American Legion Scholastic Medal of Honor
Penn State Chancellors Circle of Honor
Penn State Faculty award for Best Engineering Student
Traina Memorial Scholarship for outstanding academics and community service
Penn State Minority Award and Scholarship for outstanding minority
Robert & Sandra Poole Schreyer Honors College Scholarship in Engineering.